Direct measurements of electronic ground state ro-vibrationally excited D_2 molecules produced on ECR plasma-facing materials by means of VUV-FT absorption spectroscopy

S. Béchu, J.L. Lemaire, L. Gavilan, S. Aleiferis, V. Shakhatov, Yu.A. Lebedev, D. Fombaron, L. Bonny, J. Menu, A. Bès, et al.

Direct measurements of electronic ground state ro-vibrationally excited D_2 molecules produced on ECR plasma-facing materials by means of VUV-FT absorption spectroscopy

S. Béchu,[1, a)] J. L. Lemaire,[2, b)] L. Gavilan,[3] S. Aleiferis,[4, c)] V. Shakhatov,[5] Yu. A. Lebedev,[5] D. Fombaron,[1] L. Bonny,[1] J. Menu,[1] A. Bès,[1] P. Svarnas,[4] and N. de Oliveira[6]

[1)] *Laboratoire de Physique Subatomique et de Cosmologie, Université Grenoble-Alpes, CNRS/IN2P3, F-38026 Grenoble, France*

[2)] *Institut des Sciences Moléculaires d'Orsay (ISMO), CNRS - Université Paris-Sud (UMR 8214), 91405 Orsay, France*

[3)] *Space Science & Astrobiology Division, NASA Ames Research Center, Moffett Field, CA 94035, USA*

[4)] *High Voltage laboratory, Electrical and Computer Engineering Department, University of Patras, Rion-Patras 26504, Greece*

[5)] *Topchiev Institute of Petrochemical Synthesis, Moscow 119991, Russia*

[6)] *DESIRS beam line, Synchrotron SOLEIL, Saint Aubin 91192 Gif sur Yvette, France*

Ro-vibrationally excited molecules of deuterium are involved in non-equilibrium chemical reactions in divertor region of tokamak, molecular assisted recombination, or in neutral beam injector to produce negative ion, dissociative electron attachment, for fusion plasmas. These molecules produced both in a plasma volume and on surfaces are no longer in their electronic ground state $X\ ^1\sum_g^+(v" \geqslant 0, J")$ and populate non-uniformly different vibrational (v″) and rotational levels (J″). The high resolution VUV Fourier Transform spectrometer of the DESIRS beam line (SOLEIL synchrotron) is applied to directly scrutinize the ro-vibrationally excited levels of the D_2 ground state from $v'' = 0$ to 10 and J″ up to 8 in an electron cyclotron resonance (ECR) cold plasma. This is performed for different plasma-facing materials, i.e. quartz, tantalum, tungsten, and stainless steel, in order to compare their relative impact in molecular excitation through recombinative desorption from surfaces. A significant effect of these materials on the absolute distribution of the vibrationally states has been found above $v'' > 3$. The experimental detection limit for Quartz is $v'' = 7$ whereas tungsten and stainlees steel excite the molecules up to $v'' = 9$ and tantalum up to $v'' = 10$. The use of a bare, temperature-controlled surface of Quartz as a reference, compared to metallic surfaces, allows us to determine the relative production of these excited levels. The recombinative desorption rate on tungsten and stainless steel compared to quartz is ∼2.6 higher and reaches ∼5 for tantalum.

Keywords: Deuterium, ro-vibrationally excited states, recombinative desorption, VUV absorption spectroscopy, Fourier transform, ECR plasma

1. INTRODUCTION

1.1. Interest of ro-vibrationally excited molecules

Rovibrationally excited hydrogen (H_2), deuterium (D_2) and hydrogen deuteride (HD) molecules in their electronic ground state $X\ ^1\sum_g^+(v" \geqslant 0, J")$ are of interest to many fields.

In astrophysics, activation barriers of chemical reactions between hydrogen and primary components of the interstellar medium (atomic species such as He, Li, C, N, O, and diatomic molecules such as CO, OH, NH to name a few) can be overcome or diminished when the internal energy of the excited hydrogen molecule is considered[1,2]. The rotational (J″) and vibrational (v″) excitation of molecules play an important role in the chemistry and in the thermal balance of interstellar clouds[3].

In the hot plasmas of fusion reactors, the molecular assisted recombination (MAR) regime decreases the positive ions flux at the divertor targets by different mechanisms where ro-vibrational levels of the molecules in their ground state are involved[4]. The internal energy distribution of molecules over different vibrational quantum levels v″ is fundamental for the theoretical modeling of the MAR mechanism in order to decrease the power load on the divertor targets in tokamak[5] .

In the cold plasma physics, the importance of both ro-vibrationally excited levels and electrons of weak energy has been stressed by Allan *et al.*[6] to explain the anomalous production of negative ions H^-, D^- in plasmas: when cold electrons (< 1 eV) collide with these excited molecules (eq. 1), the incident electrons are captured by D_2, and first a Rydberg-excited electronic state of D_2 is formed prior to the creation of a negative ion and a D-atom[7,8]. The yield of this reaction, named dissociative electron attachment (DEA), depends strongly on the vibrational level of the ground state molecules[9]: the cross-section increases from 3.11×10^{-28} to 1.08×10^{-21} m^2

[a)] author to whom all correspondences should be addressed: bechu@lpsc.in2p3.fr

[b)] previously at Observatoire de Paris (LERMA).

[c)] current address: Institute for Nuclear and Radiological Science and Technology, Safety and Energy, NCSR Demokritos, 15310 Agia Paraskevi, Greece; EUROfusion consortium, JET, CCFE, Culham Science Centre, Abingdon, Ox14 3DB, UK.

for increasing vibrational level v″ = 0 to 6. The knowledge of the vibrational distribution function (VDF) of these quantum levels is therefore essential to evaluate the DEA yield.

$$D_2(X^1\sum_g^+, v" > 0) + e_{cold} \rightarrow D_2^-(^2\sum_u^+) \rightarrow D^-(1s^2) + D(n = 2) \qquad [DEA\ process] \tag{1}$$

Other negative ions such as O^-, N_2O^-, F^-, etc. observed in the semiconductor etching processes[10] are also produced by DEA[11,12] between cold electrons and rovirationally excited molecules. Negative ions could be employed to limit damages induced by charging effects inside the etched patterns[13]. A high density of negative ions obtained via DEA is also of interest in negative ion sources: for high intensity particle accelerators[14,15], negative H^- ions charge-exchange injection has allowed a noticeable increase of the emittance and of the beam intensity compared to proton injection[16,17]; and in the neutral beam injectors (NBI) of a tokamak[18,19], the acceleration of negative ions prior to their neutralization can transfer enough energy to neutrals to satisfy the Lawson criterion, the theoretical condition for the ignition of the fusion reaction[20].

Until now, high density beams of negative ions have been created on ceasiated surfaces: neutral atoms (D_0) are backscattered from the surface as negative ions (D^-). The lower the work function of the surface, the higher the fraction of the backscattered D^- (Fig. 1). A uniform and intense ion beam is mandatory for the operation of ITER (International Thermonuclear Experimental Reactor) at full power (H^- beam at 0.87 MeV and 46 A, D^- beam at 1 MeV and 40 A both during 3600 s) and for DEMO pre-industrial reactor (D^- beam at 1 MeV and 40 A both during 3600 s)[21]. However, the future use of caesium (Cs) would be problematic as it could escape the ion source between pulses and could diffuse into the accelerator stage and could be among the factors which promote beam halo effects (aberration). The use of Cs also requires regular maintenance of the ion source on ITER injector, which will be quickly activated and such operations will have to be done via remote handling. Hence, alongside theoretical works[22,23] and experimental studies[24–27] (close to full scale for some of them) devoted to optimise and to secure the use of caesium in negative ion sources, theoretical and experimental studies[18,28] (at laboratory scale) on "Cs-free" ion source have been also undertaken. N-doped surfaces of diamond[29] or barium[30,31] can theoretically produce negative ion beams (Fig. 1), but their yields remain low[28]. Hence, the possibility to enhance the production of ground state ro-vibrationally excited molecules and negative ions, are of great importance for a large field of applications. So is the ability for their measurement.

1.2. Creation of ground state ro-vibrationally excited molecules

The excitation of deuterium molecules in a plasma is a complex process driven by electrons and involving a neutral/ionized mixture of molecules and atoms spread over several electronic states in non-thermal equilibrium[32]. Depending on the energy of the colliding electrons and molecules, they are either dissociated through several possible mechanisms or brought to an excited singlet or triplet state (the latter leading to the dissociation) as summarized in Fig. 1. Fig. 2 shows the potential energy diagram of D_2 and D relevant to this work.

The principal mechanisms for the creation of $D_2(X\ ^1\sum_g^+, v")$ molecules are given in table I. Volume reactions occur in the plasma bulk far from surfaces containing the plasma. Mosbach[33] and Capitelli *et al.*[34,35] have highlighted the e-impact excitation (E-V) reaction as the most probable route to the volume production of $D_2(X\ ^1\sum_g^+, v" > 0)$ molecules when D-D recombination and losses are considered (Fig. 1). E-V consists of excitation by hot electrons ($T_e > 10$ eV) from the v″ = 0 level of the ground state (X) to the first excited electronic state (B) from which the decay to the electronic ground state is optically allowed[32]. The cross section for the excitation of this first state is higher than for the other states. This makes this B state as the main contributor to the vibrational excitation[36]. Contributions of other singlet states (C, EF, ...) to the E-V excitation are estimated to be about 25%[37].

However, surface reactions are also of great importance for the production of ground state ro-vibrationally excited molecules. Table I presents the most probable surface reactions occurring at low pressure, i.e. Auger[38] and recombinative desorption. At low pressure and in a partially ionized plasma, the D-atom density is nearly two orders of magnitude higher than D_2^+. Hence, in the following analysis, only the recombinative desorption from surfaces will be considered. This surface reaction occurs when atoms impinge on a surface and either react immediately or diffuse for a short time before they react with already adsorbed atoms[39,40]. Surface mechanisms such as Langmuir-Hinshelwood[41], Eley-Rideal[42,43] and Hot-atom[35,44,45] also result in ro-vibrationally excited ground state molecules as those produced by the reactions occurring in the plasma volume but they lead to different vibrational distributions.

Numerous theoretical and experimental studies have been published mostly for graphite and

tungsten[34,43,46–48] and tantalum surfaces have been also employed in filamented plasmas[49,50] or in electron cyclotron resonance (ECR) plasmas[51].

1.3. Indirect and direct measurements of $X\ ^1\sum_g^+(v",J")$

Many direct and indirect plasma diagnostic techniques are available. Indirect methods only probe by-products of reactions involved in the formation of ground state ro-vibrationally excited molecules. Direct methods specifically measure the population of ground state ro-vibrationally excited molecules that we are interested in. Both of these methods will be described in the following sections.

1.3.1. Indirect methods

A first indirect method, described by Hall *et al.*[50] and developed by Markelj *et al.*[52], is based on the dissociative electron attachment (DEA) to probe hydrogen and deuterium molecules in their ground state. In a cooled gas cell, molecules are dissociated on the surface of a heated filament (made of tungsten or tantalum) at 0.13 μbar. Molecules of different vibrational levels are produced on the gas cell walls by recombinative desorption of atoms. An electron gun, delivering an e-beam with a 0.3-0.4 eV resolution from 0.01 eV up to 20 eV, probes the vibrational levels through the DEA mechanism which converts these molecules into negative ions. The yield of H^- is measured by a quadrupole mass-analyzer as a function of the electron energy in the 0 - 5 eV range. This experimental setup does not allow to probe the different rotational molecular levels[52–54]. This method has been employed to demonstrate the effectiveness of the recombinative desorption on different materials (Cu, W, carbon) both for H_2 and D_2 molecules[52,53].

Other authors[49,51] use laser-photodetachment of negative ions to indirectly probe these excited ro-vibrational levels. Multiple undetermined densities of species are involved in these measurements: populations of different ro-vibrational levels, densities of cold electrons and of atoms.

An additional, indirect method employs optical emission spectroscopy measurements of the Fulcher-α band (transition d $^3\prod_u \rightarrow$a $^3\sum_g^+$, see Fig. 2) emitted in the visible spectral range (600 to 650 nm)[55–58]. The main interest of this method, based on the pioneer work of Lavrov[59,60], is that it deals only with visible spectroscopy. However, based on several assumptions, this method requires the correct interpretation of the experimental results obtained via optical emission originated from the triplet state, whereas its objective information concerns the ground singlet state.

1.3.2. Direct methods

Many authors have used laser-based high resolution methods to perform direct measurements of v″ densities:

• Multi-photon ionization (MPI), using two-photon excitation through E,F states and a third photon for ionization Marinero *et al.*[61] detected J″ levels of v′ = 0, 1 and 2 for H_2, by measuring rotational temperatures close to the Boltzmann distribution. Using resonantly-enhanced MPI (REMPI) Eenshuistra *et al.*[62] in a (3+1) REMPI scheme have obtained absolute densities of final quantum states v″ from 1 up to 5. Lemaire *et al.* sampled D_2 molecules (desorbed after formation by atoms recombination on a 10 K surface) in the v″ = 4 exited level of the ground state with (2+1) REMPI coupled with TOF mass spectroscopy[42].

• Vacuum ultraviolet (VUV) laser absorption spectroscopy, based on the advent of VUV generation by non-linear third harmonic generation (3HG)[63] and four-wave frequency mixing (FWSM), allows absorption spectroscopy without using a monochromator thanks to the laser narrow spectral bandwidth (0.27 cm^{-1}) and high radiation intensity ($\sim 10^9$ photons/pulse). Stutzin *et al.*[64,65] followed by Wagner *et al.*[66] employed this diagnostic, between 0.6 and 16 μbar, in a multicusp ion source in which the commonly used heated filaments are replaced by LaB_6 cathodes.

• Coherent anti- Stokes Raman spectroscopy (CARS) technique, has been used by Péalat *et al.*[67] to study the ro-vibrational population of H_2 and D_2 in a magnetic multicusp discharge where v″ = 3 was observed for D_2 molecules. Meulenbroeks *et al.*[68] measured the density of H_2 molecules in different J″ levels of v″ $\leqslant$2 in an expanding Ar-H_2 plasma from a thermal arc source. Hassouni *et al.*[69] have also employed CARS technique and the refined modeling to describe the chemistry of an RF (13.56 MHz) plasma discharge at medium pressure (1.3 mbar) with the recombination coefficient of H atoms on the surface as adjustable parameter.

• Laser Induced Fluorescence (LIF) with VUV-laser beams generated via stimulated anti-Stokes Raman scattering (SARS) in cold high-pressure hydrogen Raman cell has been employed by Mosbach *et al.*[70] in a filamented magnetic multipole plasma and successively by Vankan *et al.*[71] and Gabriel *et al.*[72] in a cascaded arc plasma. The main drawbacks of this method are its limitation in energy coverage due to the necessary use of either LiF or MgF_2 optical components to sort different Raman orders and its inability to probe the B-X(v′ = 0, v″) transitions for v″ < 2, missing in particular the important case of v″ = 0. Also, the calibration of LIF intensity in absolute scale requires additional measurements with another neutral gas (Kr in the case of VUV-LIF) at well-known density. The complex LIF emission spectra, obtained when laser emission lines interact with the probed plasma, requires sophisticated modeling to be analyzed.

• Photon-induced fluorescence spectroscopy (PIFS), using synchrotron radiation, has been employed by

Schmidt *et al.*[73] to probe through the dispersed fluorescence the vibrational progressions from the Lyman band of H_2 for v′ up to 13 and v″ from 6 to the dissociation limit.

• Synchrotron radiation (SR) has been employed by Béchu *et al.*[51,74] to performe preliminary experiments using high-resolution VUV-absorption in a hydrogen plasma using the DESIRS beam line of the SOLEIL synchrotron to directly and selectively probe the ro-vibrationally excited H_2(v″,J″) molecules in the ground state H_2(X). The monochromatized SR enters in the plasma chamber where it is selectively absorbed. The transmitted light was detected by a solar blind VUV photomultiplier. In addition, to eliminate the stray plasma light, the SR was chopped by a tuning fork, oscillating at a constant frequency f = 130 Hz, for phase-sensitive detection. Nonetheless, the number of the observable bands was limited to five transitions B(v′ = 0) ← X(v″ = 2 to 6) and in the best case restricted from J″ = 0 to 4 or 5.

Although indirect methods are less expensive than direct ones, they provide less insight. Direct methods using VUV laser are rarely carried out due to the rather complex and expensive diagnostic required and the sparse results obtained. In this work, the unique combination of a SR source and Vacuum Ultra Violet Fourier Transform Spectrometer (VUV-FTS) allows a direct and accurate measurement of the density of the ro-vibrationnal components of the D_2 molecule in its ground state.

1.4. Interest of an ECR plasma source for fundamental studies on recombinative desorption.

Recent results have shown that a caesium-free (Cs-free) Helicon plasma reactor, named RAID, produces at 3 μbar and 5 kW a negative ion density of $\sim 2 \times 10^{16}\ m^{-3}$ in H_2 plasma and $\sim 1.75 \times 10^{16}\ m^{-3}$ in D_2 plasma[75]. In comparison with BATMAN[25] ion source, the one eighth scale prototype of the future negative ion source of ITER tokamak, the same density of H^- is obtained with an input power of 40 kW when using caesium[76]. Kurutz *et al.*[28], in an inductive plasma, do not observe a significative effect of recombinative desorption over direct ionization on ceasiated surface to produce negative ions via DEA. Hence, this experimental result obtained with an helicon antenna, in the RAID reactor, is very promising and demonstrates the possibility to produce a high density of negative ions in Cs-free plasmas on a length of more than one meter which could be relevant as a future negative ion source for plasma fusion[77]. However, the RAID reactor size does not allow the possibility to be set up on the DESIRS beam line. Therefore, we use an ECR plasma as a substitute to the helicon plasma. Five ECR dipolar plasma sources implemented in PROMETHEUS-I reactor[78] give similar n_i^-/n_e density ratio as RAID, 0.25 and 0.22, respectively, at the same working conditions. Even though the absolute density in the PROMETHEUS-I[79] reactor is lower $\sim 5 \times 10^{15}\ m^{-3}$ than in the RAID reactor, it is obtained at lower input power, 0.9 kW instead of 5 kW. The ECR source[79,80] presented in Figs. 3a and 3b produces a plasma which is similar to the helicon plasma produced in the RAID reactor: two main zones are distinguishable, i.e. the ECR coupling zone (very bright) where electrons are heated by the ECR phenomenon and a diffusion plasma (glowing zone with weaker brightness) where electrons are colder[81]. Such a plasma source also presents the following advantages:

▶ the plasma source has already shown a high stability in a precedent study[51].

▶ the size of the plasma source[80] is smaller than the Helicon antenna[82].

1.5. Paper organization

This manuscript is organized as follows: in the preceeding sections a summary of the plasma spectroscopy and of the previous works in the context of the present study are provided (Section 1). Thereafter some details of the experimental setup and data recording procedures are presented (Section 2), followed by a step-by-step description of the data analysis (Section 3) that was used. The study continues with a detailed description of the final results (Section 4), focusing more on the ro-vibrational populations in the D_2 X $^1\sum^+$ electronic ground state and the comparison between different materials for the reactor walls. The paper ends (Section 5) with a discussion and concluding remarks.

NB: Throughout this paper we will use the following notation for concision: BX02 (or BX 0-2) describes, for instance, the transition B(v′ = 0)←X(v″ = 2). If necessary, when v″ ⩾10, we will use BXv′-10 instead.

2. EXPERIMENTAL PLASMA SETUP AND DATA RECORDING

The experimental setup is composed of two main parts: a reactor containing the ECR plasma source and the VUV-FT spectrometer.

2.1. The reactor

The detailed description of the experimental setup used for this study has been reported in a previous paper[51]. We are reporting here its main characteristics and improvements related to the present work.

2.1.1. Plasma chamber

The plasma chamber (Fig. 3a) contains a Quartz cylinder (aluminosilicate glass - Schott^{TM} 8250) whose inner surface can be partially covered (66 %) by a foil (0.1 mm thick) of the studied material. Three different materials have been investigated throughout this study: tantalum (Ta), tungsten (W), stainless steel (SS) and Quartz (Q) as the reference surface. Consequently the plasma faces a material either of low ($\gamma \sim 0.004$ at 290 K for Quartz)[83,84] or high recombination probability ($\gamma \sim 0.5$ at 240-300 K for metallic surfaces)[85]. This chamber is also closed on both ends with disks of Quartz (the investigated material is only set at one end). The Quartz cylinder is permanently placed within a copper cylinder, cooled at a regulated temperature of 283 K. The copper cylinder is housed in a stainless steel cylinder which is the external wall of the reactor. The inner dimensions of the Quartz tube are 124 mm in diameter and 220 mm in length. The plasma reactor is installed upstream of the VUV-FTS instrument and inserted between two different sets of differential pumping. First, two capillaries (ϕ 8 mm, 50 mm length) separate both sides of the reactor chamber from a set of differential pumping chambers (equipped with 2×50 l/s turbo-pumps). Inside this first set of chambers the pressure is already reduced to 0.1 μbar, when running the reactor at 8 μbar. The SR beam goes through a second stage of differential pumping chambers (equipped with 2×500 l/s turbo-pumps) located on one side at the SR beam exit and on the other at the FTS entrance. In addition, two sets of rectangular tubes shaping the incident beam (8×5 mm^2, 150 mm long) complete the differential pumping system allowing a final pressure of 10^{-7} mbar, for 8 μbar inside the plasma source chamber, without perturbing the ultra high vacuum of the FTS and the synchrotron beam-line. All these differential pumping systems are additional to the main turbo-molecular pump (800 l/s), directly installed on the plasma chamber. This pump is slowed down in operation in order to maintain a suitable pressure inside the reactor and to reduce the D_2 gas consumption.

A cleaning procedure (D_2-Ar / 80-20% plasma-ON) is done after each surface material change. This procedure is followed by a 15 minutes warming up period, in a pure D_2 plasma, to ensure plasma stabilization and thermal equilibrium. The base pressure is always below 6×10^{-4} mbar before starting plasma ignition and measurements. In a previous study[51], we quantified the following relative uncertainties: plasma density n_e of ±1.4%, plasma potential V_p of ±0.6%, and electron temperature T_e of ±1.8%.

2.1.2. ECR plasma source

The plasma source[79–81] consists of an opened coaxial line where microwaves propagate up to a water-cooled cylindrical encapsulated permanent magnet. The ECR coupling condition (0.0875 T) between the microwave electric field (2.45 GHz) and electrons is fulfilled close to the magnet where, electrons in the 10 to 30 eV energy range are generated. Figure 3b shows a side-on view of the end of the plasma source surrounded by the plasma. The ECR coupling zone, between the plasma electrons and the alternative electric field (2.45 GHz), is the brightest zone of the glowing plasma. The microwave power is supplied by a solid state microwave generator (SAIREM®), with a maximum power of 450 W. All experiments are performed at 150 W. The plasma source has its own tuner for the impedance matching (less than 1% of reflected power is acceptable during operation). The SR beam light probing the plasma along the reactor inner diameter (124 mm) is located 25 mm from the top of the plasma source.

2.2. The VUV-FTS at the DESIRS beamline

The spectroscopic diagnostic method employs the powerful FTS capabilities in a large VUV spectral range available on the beam-line DESIRS (Dichroïsme Et Spectroscopie par Interaction avec le Rayonnement Synchrotron) of the SOLEIL synchrotron facility (Saint Aubin, France). The VUV-FTS, described in detail in previous publications[86–88], is used to diagnose D_2 molecules, by absorption spectroscopy. The VUV-FTS coupled to the undulator-based DESIRS SR is able to provide simultaneously a high spectral resolution (maximum resolving power $R = \lambda/\Delta\lambda \sim 10^6$), a high accuracy of the energy scale over a large spectral range (5 eV to 30 eV$\sim$ 250 to 40 nm) as well as a large flux ($\sim 10^{15}$ photons/s). The VUV-FTS interferometer is based exclusively on reflective optical surfaces giving access to the large UV-VUV spectral range offered by the beamline, provided no window is inserted. The acquisition time (10 to 30 min depending on the required resolution and S/N) is much shorter compared to tunable VUV laser absorption spectroscopy for the production of a complete spectrum over a bandwidth of $\sim$5000 cm^{-1} giving simultaneous access therein to all observable atomic or molecular signatures. For all these reasons, the present study provides a larger set of results than any other before.

In this work, which has not been performed up to date in a D_2 ECR plasmas with such a high spectral resolution and accuracy, we probe the $B\ ^1\sum_u^+(v' \geqslant 0, J'') \leftarrow X\ ^1\sum_g^+(v'' \geqslant 0, J'')$ transitions directly in the plasma volume for different plasma-facing surface materials. Inspired by previous studies[89,90], we have employed an enhancement to conventional VUV-absorption spectroscopy: the VUV-FTS which allows access to ultra high resolution in the far VUV spectral region, but with a major advantage compared to VUV laser-based absorption spectroscopy which is the relatively fast recording of a broad band spectrum.

2.2.1. Absorption spectroscopy of D_2*(v",J") molecules

Our entire setup is windowless in order to record spectra in the far VUV range (below 105 nm). We examine the absorption transitions from the ground state $X^1\Sigma_g^+$ to the singlet $B^1\Sigma_u^+$ state, also called Lyman band. This work is restricted to the BX transitions, less crowded than the CX ones, thus avoiding line blending effects. Even if also present and observed in absorption in the VUV range, the atomic Lyman series data will be presented in a forthcoming paper as they require additional emission data to be taken in the laboratory in identical plasma conditions.

The quasi-continuum light source is provided by an undulator that delivers a quasi gaussian-shaped illumination with a FWHM of about 7% of its central frequency. The high harmonics produced in the undulator are suppressed by a rare gas (Xe or Kr) flowing inside a dedicated gas filter chamber located upstream of the FTS experimental branch. We worked with photons in the 64000-96000 cm^{-1}(7.93-11.9 eV) energy range which covers a large number of BX transitions between v′ and v″ ranging from 0 to 10. Ten settings of the undulator are used to cover this broad energy range which is required due to the large spacing between vibrational bands for D_2, as shown in Fig. 4. Thanks to the overlap between spectra recorded with nearby undulator settings and also the high signal to noise ratio in the half maximum amplitude of each quasi-continuum, it is possible, to improve the accuracy of the recorded data in the intermediate spectral regions by averaging the spectra obtained with adjacent undulator setting in their common parts with amplitudes ∼40% of their maximum.

The SR beam is focused in the vertical plane on the entrance slit (100 μm) of the FTS. The area probed by the beam in the reactor, is located ∼ 40 cm upstream from the slit. A bottle of D_2 isotopically purified gas (Air Liquide, 99.997%) is used. However, small traces of H_2 are detected, originating as impurity in the rare gas used in the gas filter, but not interfering with the D_2 spectra. The gas is ionized/excited/dissociated by an ECR elementary dipolar plasma source[79,81]. In windowless mode, the above mentioned four series of capillaries and apertures are dedicated to keep the pressure on both sides of the reactor compatible with those in the beamline and in the FTS apparatus.

A D_2 gas pressure of 8 μbar in the reactor and a plasma excitation of 150 W are used as constant plasma conditions throughout the whole set of records. The pressure was chosen so that the column density of D_2 absorbs down to ∼22% of the continuum, avoiding saturation (optical depth lower than 1.5) but allowing the observation above the noise level of the BX0v″ transitions with the highest v″ possible. In order to verify that lines are not saturated, we have recorded two spectra in the absence of plasma at 8 and 0.8 μbar, and look at BX$v'0$ transitions, confirming that up to optical depth of ∼1.5 both signals are proportional to the pressure.

We have recorded a total of 58 vibrational bands each including between 16 to 6 rotational lines (those with less than 6 lines have not been considered). Experiments are performed with four different wall materials. Including ten additional spectra recorded at 0.8 μbar for BX00 without plasma, the total of lines analyzed amounts to about 3200. Careful checks to detect potential blends were performed throughout the data analysis procedure.

The unique resolving power of R ∼ 150000 has been used throughout the whole set of records, allowing the clear identification of lines separated by 0.5 cm^{-1} (around 75000 cm^{-1}) to 0.6 cm^{-1} (around 90000 cm^{-1}). Atomic lines of Kr and Xe in the gas filter enable the FTS calibration procedure. Due to their narrow line-widths, these atomic lines present a *sinc* function (sine cardinal, $sin(x)/x$) line shape characteristic of the Fourier transform (see Fig. 5). The measured FWHM of the Xe absorption line (produced in the gas filter, a capillary filled with high purity Xe gas) in the middle of the region of interest at 77185 cm^{-1} is 0.54 cm^{-1} while its Doppler FWHM is 0.083 cm^{-1} at 293 K. These results confirm the actual theoretical instrumental line width set for the FTS during this campaign. This value can be further refined by fitting the *sinc* function secondary maxima positions in addition to its FWHM. For comparison, a nearby H_2 line (at 78436 cm^{-1}) whose line profile is also the convolution of its Doppler profile with the apparatus function displays a FWHM of 0.88 cm^{-1} (see Fig. 5a), showing a quasi-complete cancellation of the *sinc* oscillations in the line wings. Samples of D_2 lines are given in Fig. 5b with the plasma ON for the BX31 P4 line and in Fig. 5c both with and without plasma for the BX00 R2 and P1 lines separated by 1.44 cm^{-1}. All these lines, at frequencies around 90000 cm^{-1}, present a FWHM of 0.71 cm^{-1}, relatively close to the *sinc* FWHM value. Simulations of convolution of a gaussian with the *sinc* determined above allow us to correct the measured values. Then a FWHM of 0.71 cm^{-1} for D_2 corresponds to a 0.63 cm^{-1} FWHM gaussian, while for H_2 the wider value of 0.88 cm^{-1} corresponds in fact to a true gaussian FWHM of 0.86 cm^{-1}. In every scan, all D_2 lines are fitted by *sinc*-convoluted Gaussian curves.

Recording a raw interferogram at the chosen resolution takes about one minute. Thus an interferometer scan is repeated at least twelve times to increase the S/N ratio. A key element of this work is the need for the almost perfect stability of the plasma characteristics during the data acquisition. The two most critical elements are the pressure stability, ensured by a regulator, and the microwave power stability. Several reference spectra taken at different days have proven that these requirements were fulfilled. In addition, the stability of the plasma source is checked with a small integrated spectrometer coupled to an optical fiber installed on a side-window of the plasma chamber. This setup is used to observe the emission intensity of the Balmer series, together with repetitive records of the Fulcher bands during each VUV-FTS scan. All spectra are recorded at room temperature,

293 K.

2.2.2. Emission spectroscopy diagnostics tools

As deuterium molecules are excited to the B electronic state in the plasma, we could observe, in principle, the emission due to its relaxation to the X state as UV or VUV photons. Test experiments have shown that the plasma emission alone, in the absence of the SR beam probe, is not detectable thus not perturbing the absorption signal when the SR probe is on. This is explained by: a) the high directivity (or spatial coherence) of the undulator-made SR continuum compared to the much less bright and 4π spread plasma emission and b) the present reactor/entrance slit geometry (distance of $\sim$1 m between the plasma chamber and the 100 μm FTS entrance slit). The net result is that the plasma fluorescence is, in our case, well below the detection limit of the FTS.

However, D_2 emission spectroscopy can be performed by the analysis of transitions between triplet electronic states emitting in visible. In particular between the triplet states $d^3\Pi_u$ and $a^3\Sigma_g^+$, which gives rise to the so called Fulcher(α) bands. To this end, we use a medium resolution spectrograph in the 600 - 650 nm range. This diagnostic was used by some authors[55–58] as an alternative indirect determination of rotational populations of molecular hydrogen in a plasma. This measurement is mentioned here for the sake of completeness but the analysis of its results and the comparison to our direct populations characterization will be the subject of a forthcoming paper.

3. DATA ANALYSIS

3.1. Introduction

For the pure D_2 gas at room temperature, all the population lies in the ground state $X^1\Sigma_g^+(v''=0,J'')$ levels. Thus its absorption spectrum is only composed of BXv′0 lines connected to this level as shown in Fig. 6a. These lines are later used for population calibrations. When the plasma is ON, we observe both a reduction of the population in the X($v''=0$) vibrational level together with a much more crowded absorption spectrum as shown in Fig. 6b. This is due to the dissociation and electronic excitation induced by electronic collisions as well as to the recombinative desorption of the deuterium atoms on the walls of the reactor chamber. Indeed, in a plasma, many allowed singlet transitions between ro-vibrationally excited levels of the ground state and excited electronic states (B, C, B′, D″, etc.), the so-called hot bands, are observed as well as triplet-triplet transitions.

As already noted in Fig. 5, we observe that for all lines in the BXv′0 bands, their FWHM linewidths, without and with plasma, are identical, thus showing no effects due to the plasma heating. The FWHM is the same for all BXv′v″ transitions. This common linewidth corresponds to a D_2 translational gas temperature of $\sim$330 $\pm$ 10 K.

The aim of this work is to compare the impact of different plasma-facing materials on the recombinative desorption and to compare these results with ro-vibrationnal excitation of D_2 molecules in the ground state when a bare Quartz surface is used. To this end, we could separately measure each BX0v″ absorption spectra between different ro-vibrational levels of the X state up to the highest v″ possible (i.e. $\leqslant 17$, the dissociation limit[32]) and the B state lower level $v'=0$. Nevertheless, because the FTS gives access to a multitude of vibrational bands in a given spectral range within a single scan, we are able to simultaneously obtain the complete dataset for all BXv′v″ transitions. Although this makes the data analysis more complex, it also allows a crosscheck between bands and to improve the coherence and quality of our spectroscopic analysis.

As already mentioned, 58 bands have been observed and recorded in absorption which are reported in Table II. We also report in Table III, for each vibrational band, the position in wavenumbers of the first rotational line R0. Some of the observed vibrational transitions are favorable due to their Franck-Condon (FC) factors for which rotational $J''\leqslant 8$ are measured. This means that 16 rotational lines (R0 to R8 and P1 to P7) are sufficient, in our plasma conditions, to acquire the total population of the vibrational level considered. Some bands, partially subject to saturation, are also indicated in Table II. The FC coefficients used in the analysis are obtained from Fantz & Wünderlich (2006)[32] and are presented in Table IV.

3.2. Step by step analysis

• The first step in the analysis is to convert the raw absorption spectra (intensity I) shown in Fig. 4 into optical depth spectra. This is done by fitting a baseline continuum I_0 in order to calculate the optical depth, τ, $\tau = \ln(I_0/I)$. This continuum appears in the figure as a colored solid line on top of the spectrum. According to the Beer-Lambert law the optical depth is correlated to the thickness and physical properties of the attenuating medium by $I(\nu) = I_0(\nu)e^{-Nx\sigma_{meas}(\nu)}$ where N is the density, x the column length and $\sigma_{meas}(\nu)$ is the measured absorption cross section of the species. σ_{meas} includes the effect of the finite instrument resolution. We then consider here the convolution of a gaussian (neglecting the small lorentzian contribution of the natural width) with the instrumental *sinc* function. As the effect of the apparatus function on each frequency ν is the same for all D_2 lines and as all lines can be fitted by a *sinc*-convoluted gaussian of unique FWHM (subsection 2.2.1), we will consider for each line the optical depth peak, $\tau_{max} = \ln(I_0/I_{max})$, as the final data.

• The second step is to identify the observed spec-

tral lines and to check for possible blends or overlaps between different bands. For this we refer to the MOLAT Atomic and Molecular database available at https://molat.obspm.fr/ in the section "VUV Spectra of Small Molecules" for hydrogen and deuterium based on the work of Roncin & Launay (1994)[91].

The values of the optical depth peaks are plotted in graphs in order to check for possible blends. For example, the set of Figs. 7 shows, for a subset (v″ = 0, 2 and 3) of the BX0v″(v″ = 0 to 9) transitions, the peak optical depths for the R- and P-branches versus the corresponding transition energies. The first figure of this set concerns the pure D_2 gas without plasma excitation, and all the others when the plasma is ON. We notice an unfortunate blend of BX00 R1 (Plasma-ON condition) with the CX03 Q3 line. An approximate correction is made, in Fig. 7b, by multiplying R1(w/o plasma) with the ratio of the sum of all others R and P lines with and w/o plasma. Its incidence is negligible as its effect will be smeared out later in the J″ summation process. We notice also that due to its low FC, the BX0-10 transition is not observed while the BX1-10 and 2-10 transitions are clearly present. The same procedure is applied to all observed transitions BX v′v″ for v″ = 0 to 9 available for all v′ with v′ = 1 to 10.

It is also worth mentioning that many other transitions BXv′v″ for v′>10 and v″ between 0 and 3, lying outside of the energy range systematically recorded (64000-96000 cm^{-1}) for all surface materials, are observable in the 93000-110000 cm^{-1} range. However most of them are saturated at low J″, as it can be noticed in Fig. 4 at high frequencies in a single record for Ta, in the 101000-110000cm^{-1} range.

• The third step is to sum the R and P absorbance values with the same J″. This allows us to check on variations due either to line blending or to saturation effects. Figures 8a and 8b illustrates the case of BXv′2 and BXv′3 where the 7 values of v′ are used as labels. The shape of these curves are compared in subsection 4.3 to Boltzman distributions at different temperatures.

• The fourth step, considering that for a given v″ vibrational number all the rotational transitions to the different v′ vibrational numbers have in first approximation the same rotational oscillator strengths, consists in simply adding all the rotational contributions related to this v″ level. Such a summation, up to 16 values will increase the accuracy of our results. The validity of this assumption is presented in subsection 4.3. This summation for a given v″ level can be performed on the different v′ (e.g. BX04, BX14, BX24, ...to BX64). Our results are presented for the four materials in Fig. 9. All the apparently different values for a given v″ of the ground state X should reflect the same unique v″ population of this level, whatever v′ is considered. We recall that in absorption spectroscopy the signal observed is proportional to the population of the lower state of the transition.

• The fifth step is then to correct these line intensities by using their respective FC factors. After checking several theoretical values available in the literature, we obtain an almost perfect agreement using the values calculated by Fantz & Wünderlich[32]. This is done by finding the multiplicative value to apply to the theoretical FC factors in order to best fit, using a weighted minimization procedure, the experimental data. Fig. 9 shows the fits performed for each wall material, traced in gray color stars underneath our data points. The modeled data closely agree with the experimental data. The figure also includes the theoretical FC multiplied by suitable factor to make it more visible.

3.3. Intermediate results

Through this analysis, we derive numbers proportional to the D_2 optical depth (i.e. column densities integrated along the optical path of the SR beam), and consequently proportional to the populations in the different vibrational levels of the ground state. Table V contains the relative vibrational populations for pure D_2 without plasma and with plasma for the four wall materials. In each column, the data for the different v″ vibrational levels are normalized to the data obtained for v″ = 0 in the pure gas without plasma.

We first notice that the sum for all v″ in the ground state, when the plasma is ON, is lower than in the pure gas without plasma. This shows that molecules unaccounted-for are either dissociated into atoms, or ionized or excited in triplet states. We also notice an increase from 7 to 10 of the highest observed v″ vibrational number for wall materials in the following order: Q, W, SS and Ta. The case of v″ = 0, for which the relative populations are almost identical across wall materials, will be discussed in the next section. We also notice that for a given v″, above v″=1, the population ratio increases with the material order indicated above.

Fig. 10a shows the D_2 relative vibrational populations distribution in the $X^1\Sigma^+$ ground state without and with plasma excitation (150 W, 8 μbar) for Quartz.

4. FINAL RESULTS

4.1. Absolute D_2 molecular densities in the vibrational levels of the ground state in the plasma

The last step in the analysis is to extract from the previous integrated data the absolute molecular densities of D_2 in the vibrational levels of the ground state. To this end, we need to sort out the contribution of the different plasma regions: differential pumping regions, outer intermediate regions and inner plasma volume.

Some assumptions have to be made beforehand on the gas properties in the different regions. We mainly assume that the excited and dissociated species are constrained in the inner plasma volume, within the Quartz (bare or metal-covered) cylinder wall, along an optical path of 140

mm (quartz inner diameter and holes thickness throughout quartz and copper part). We also assume that due to collisions on the capillary walls an extremely low density of surviving reactive species (either atoms or $v'' > 0$ molecules) are present in the pressure gradient of the two differential pumping regions on both sides of the plasma chamber. This is also expected in the short intermediate regions between the outer envelope of the plasma chamber and the inner Quartz cylinder. From the setup geometry and assuming a linear pressure decrease in the first set of capillaries (2.1.1), this passive gas (labelled p.g. in Fig. 10a) accounts for 38^{+3}_{-2} % of the total signal observed in the pure gas without plasma. The contribution of the intermediate regions is in fact the largest source of uncertainty in our results. This 38% contribution to the $v'' = 0$ signal has to be subtracted from the total signal in all cases (with or without the plasma).

With the exception of molecules that are dissociated or ionized or excited in triplet states by electronic collisions when the plasma is ON and that we will refer to as process **(i)**, the missing molecules in the $v'' = 0$ level in the plasma, compared to those without plasma, are those subject to vibrational excitation transfer in $v'' > 0$ levels, either directly by means of collisions or by recombination on the wall surface, and will be referred as process **(ii)** (Fig. 1). Electronic collisional excitations contribute to populate both singlet and triplet states in the plasma. The excited singlet states can relax through singlet-singlet transitions (among them, the Lyman and Werner bands) into excited vibrational levels $v'' > 0$, process **(ii)**, and $v'' = 0$ level. The excited triplet states relax through triplet-triplet transitions (among which are the Fulcher(α) bands, d $\rightarrow$ a transitions). Molecules in the $a^3\Sigma_g^+$ state can be either re-excited by subsequent collisions or relaxed through the dissociative $b^3\Sigma_g^+$ state to give D(1s) + D(1s), consequently supplying process **(i)**. For a likely very small number of them, they can decay to the ground state X($v'' \geq 0$) due to singlet-triplet forbidden intercombination bands ($a^3\Sigma_g^+$-$X^1\Sigma_g^+$ or $c^3\Pi_u$-$X^1\Sigma_g^+$) that could be promoted by the strong magnetic field in the plasma source vicinity, thus supplying process **(ii)**. Fig. 10b summarizes, for the four materials and after passive gas (p.g.) suppression, the ratio of the different processes: the dissociated or ionized or excited in triplet states molecules, process (**i**), the ground state vibrationnaly excited molecules, process (**ii**), and the $v'' = 0$ ground state ones.

Table VI gives a final estimation of the absolute molecular densities in all v'' vibrational levels of the $X^1\Sigma_g^+$ ground state of D_2, considering **1)** a homogeneous plasma in the reactor, **2)** a gas temperature of 293 K (thus a gas density of 1.98×10^{14} cm^{-3} at 8 μbar), and **3)** after subtraction of the 38% passive gas contribution. The three last lines of the table give the percentages of molecules in a $v'' > 0$ level compared to Σ v'' and to $v'' = 0$, and the number of molecules unaccounted-for which are either dissociated into atoms, or ionized or excited in triplet states compared to Σ v''. It is worth mentioning that, the efficiency of the ECR coupling allows the production of electrons with high energy, E. When E >15.43 eV, there is the possibility that some of the D_2 molecules are directly ionized. According to Yang *et al.*[36], several reaction paths are leading either to D, D^+ or to D_2^*, then contributing for the two first to process **(i)** or to process **(ii)** for the latter.

4.2. Vibrational distribution function, vibrational temperature and comparison of wall materials

Figure 11a shows a Boltzmann plot of the vibrational distribution function (VDF) ln ($N_{v''}$) *vs*. E(v''), with $N_{v''}$ reported in Table VI and normalized to $N_{v''=0}$ w/o plasma of the D_2 ground state for the four plasma-facing materials. The data are normalized to the ground state v'' pure gas value (plasma OFF) and, due to the difference in the D_2 dissociation value for each material, shifted up to zero for $v'' = 0$. It appears that the four VDF present a quasi-identical shape on the whole range of v'', while a clear threshold is observed for all of them at $v'' = 3$. For $v'' > 3$, the main fact is that up to $v'' = 10$, the relative VDF shows larger populations for Ta than for W and SS which are themselves overpopulated compared to Q. This is correlated, as already mentioned, that no signal is observable above noise level above $v'' = 8$ for Q, while it is observed up to $v'' = 9$ for W and SS, and up to $v'' = 10$ for Ta. Before the $v'' = 3$ threshold, the partial vibrational population for $v'' = 0$ to 3 compared to the total one represents from ~99% for Q to ~96% for Ta, whereas the four curves are diverging afterwards.

In the Boltzmann plot representation of Fig. 11a, the reciprocal of the negative slope characterizes the so-called vibrational temperature of the plasma. From $v'' = 0$ up to $v'' = 3$, the VDF exhibits a quasi-linear behavior and a vibrational temperature of ~2800 K for Q, W and SS and a higher value Ta, ~3750 K. From $v'' = 3$ there is a sudden variation for all which slowly declines up to the higher v'' observed. This variation is less marked for Q (from ~6400 to ~4400 K) compared to W and SS (from ~11500 to ~5000 K) and to Ta (from ~12400 to ~5000 K). The drastic change in the vibrational temperature is more clearly observed in Fig. 11b which shows the evolution of the temperature between two adjacent v'' (a kind of derivative).

All of these VDF properties can be also observed in Fig. 12 showing the relative v'' population ratios in the ground state as a function of the wall material. The three materials are compared to Q in Fig. 12a where Ta appears to be, at $v'' = 7$, ~4.8 times more efficient than Q at populating high v'' levels and ~2.7 times for SS and W . Values lower than 1 for $v'' < 3$ indicate that the related material is less efficient in populating these levels than Q. The comparison of W and SS to Ta in Fig. 12b shows that, for $v'' = 9$, SS and W are respectively ~1.8 and ~2.6 times less efficient than Ta in populating this level. Again, the values lower than 1 for $v'' = 0$ indicate

that the related material is less efficient in populating this level than Ta.

4.3. Rotational distribution and rotational temperature

The rotational temperature of the molecular gas can be extracted from our set of measurements (obtained in the third step of 4.2) giving numbers proportional to the $N_{J''}$ rotational distribution. In the pure gas without plasma, the Boltzmann plot of the rotational distribution $[\ln\frac{N_{J''}}{g_{J''}\times(2J''+1)}$ *vs.* $E(J'')]$[45], gives for D_2 a rotational temperature of 328 ± 5 K as shown in Fig. 13a. This result is derived from measurements of all the available BXv′0 (v′ = 0 to 5) transitions performed at two pressures, 8 μbar and 0.8 μbar, in order to avoid saturation. Normalized relative populations allow us to co-add both sets and to cancel the FC factors of the different transitions.

As expected, when the plasma is ON, the Boltzmann plot shows a non-linear behavior characteristic of a non-Boltzmann distribution as shown in Fig. 13b. The general trend is fitted by a second order polynomial evolving from 333 ± 10 K for the low J″(0 to 3), similar to the plasma-OFF case, and up to ∼500 K for the higher ones shown in Fig. 13b. A linear fit for J″ = 6 to 8 gives an average temperature of 465 ± 30 K. The rotational temperature for all J″ is calculated from the derivative of this polynomial, linked to the scale of the right-side y-axis. While there is almost no difference between the four materials for low J″, there is a large spread at higher J″. Thus we present the averaged data for both high and low J″.

Fig. 8c shows for the case of pure Boltzmann distribution, the rotational distribution function for several temperatures (in the 300 to 700 K range relevant to our observations). Our results in Figs. 8a and 8b, can be estimated in light of Fig. 8c by comparing the intensity ratio of the J" distribution (and particularly between the even ones) and its slope (particularly between J″ = 3 to 4 and 5 to 6), that for all BXv′v″ observed the J″ distribution spreads from 300 to 600 K at the maximum.

This 330 K rotational temperature, in both case slightly higher than the experiment kinetic temperature (RT at 293 K), plasma-OFF condition, allows us to perform simulations of the BXv′0 rotational spectra using the classical Hönl-London factors and parity alternation. These simulations and their fits (and residuals) to the experimental spectra are shown for instance for BX00 and BX30 in Figs. 14a and 14b. Fitting the spectra when the plasma is ON would have required averaging several simulations at different temperatures with unpredictable respective amounts.

4.4. Translational temperature

For the sake of completeness, we recall here the results obtained in section 3 on the spectral linewidth of molecules and atoms, either D_2, D, H_2 or H. We have shown in Fig. 5 that all lines are well fitted by *sinc*-convoluted Gaussian functions. The FWHM characterizes an average kinetic temperature[92] of ∼ 330 ±10 K. We have only considered the Doppler broadening while neglecting the Stark and Zeeman effects due to the weak electron density ($< 10^{16}$ m^{-3}) and the weak magnetic field intensity (∼ 0.01 T) at 25 mm from the permanent magnet of the plasma source.

5. DISCUSSION AND CONCLUDING REMARKS

We will compare here our results, obtained with the VUV absorption spectroscopy, to several previous observations or theoretical calculations related to the populations of the vibrational levels in the electronic ground state.

5.1. Vibrational distribution function (VDF) and its effect on the production on D^- ions.

The threshold value observed in Fig. 11a and emphasized in Fig. 11b between a linear variation below v″ = 3, which indicates a Boltzmann equilibrium, and an overpopulated distribution of vibrational levels above has been observed by Hall *et al.*[50] for tantalum and tungsten. Stuzin *et al.*[65] also observed a linear shape of the VDF up to v″ ⩽ 5, even if, authors stress an uncertainty for the v″ = 5 level where only J″ = 1 is measured. Firstly, Hassouni *et al.*[69] highlighted the role of E-V process (see Fig. 1) in the formation of a plateau: high vibrational levels have the same production rate. Secondly, deactivation of these levels through collisions between ro-vibrational molecules and atoms (V-T processes) are equivalent for all of these levels. A higher density of atoms (i.e. low recombination coefficient) tends to decrease the vibrational temperature and to widen the plateau. The VDF that we measured here do not show a particular modification of their shape when the recombination coefficient is changed (when metallic surface partially covers the quartz surface). In Fig. 11a, a break is observed but there is no clear plateau beyond v″ = 3: higher vibrational levels (up to v′ = 10 for Ta) follow a Gaussian-like distribution with no clear plateau observed like those obtained by Yang *et al.*[36] when only E-V mechanism is considered in similar plasmas. In our case, firstly, the D-atoms density, estimated during these experimental series, is low (1%). Secondly, the role of the microwave dipolar plasma source surface made of stainless steel (element marked as d) in Fig. 3) may have been under evaluated: even if its surface is small, less than 15% of the total surface of the plasma-facing material, it lies at the nearest place from

the ECR coupling zone (see Fig. 3b). This hypothesis is validated by our own results, i.e. no difference in the T_{vib} values obtained with Quartz or metallic surfaces (T_{vib} = 2800 K) except for tantalum (T_{vib} = 3400 K), and by results obtained by Hall *et al.*[50], T_{vib} = 3400 K for tantalum and T_{vib} = 2800 K for tungsten. Stutzin *et al.*[65] mentioned T_{vib} = 4060 K and Wagner *et al.*[66] found similar vibrational temperatures between 4300 K and 5000 K. Hassouni *et al.*[69], at high pressure, measured T_{vib} = 4000 K.

If the over-populated tail of the VDF was attributed to recombinative desorption through different surface mechanisms as Eley-Rideal (E-R), Langmuir-Hinshelwood (L-H) or Hot-atom (H-a) from either chemisorbed-D or physisorbed-D atoms on surface as underlined by theoretical approaches by Morrisset *et al.*[41], Jackson *et al.*[39] and Cacciatore *et al.*[47] and experimentally by Hall *et al.*[50] and Mosbach *et al.*[33,70], it would not be possible to attribute a dominant role, to one of these mechanism, to explain this overpopulation of high v″ levels. Whatever the surface mechanism implied, its efficiency vs. volume mechanism (E-V reaction) for the production of high v″ levels (v″ > 3) is highlighted in Fig. 12. For v″ = 7 level recombinative rate is almost 5 times higher with Ta compared to quartz condition. The same behavior is observed with other metallic coverage (W and SS) to a lesser extent.

5.2. Distribution of energy over rotational and translational of the $D_2(X^1\sum_g^+)$ molecule

The rotational temperature is commonly attributed to the kinetic gas temperature[56,93,94] and depends on the experimental conditions. Gabriel *et al.* mentioned rotational temperature in the 3000-4000 K range[95] while Briefi *et al.* indicated a two-temperature Boltzmann distribution with a low (564 K) and a high (5440 K) component[56] and Wagner *et al.*[66] showed up lower rotational temperature, 380 K. In our reactor, in plasma-OFF condition it appears slightly above the temperature of the temperature-regulated walls of the reactor (283 K). In plasma-ON condition, it is surprisingly low even if at low pressure (8 μbar) and low electron density ($\sim 3\times10^{15}$ m^{-3}) energy transfer between electrons and neutrals through inelastic collisions is weak[96]. Péalat *et al.*[67] measured similar rotational temperature in a plasma of analogous density and highlighted the effect of passive gas surrounding the plasma, mentioned in 4.1, on the rotational temperature of the low ro-vibrational levels (v″ = 0, J″ ⩽ 3) attributed to the plasma volume. Over population of high rotational levels, J″ > 5, the rotational temperature is close to 465 K. For these higher rotational levels, the passive gas effect is negligible due to a very small population outside the plasma volume. Close comparisons between theoretical Boltzmann distributions and VUV absorption spectra demonstrate a limited rotational temperature spreading within a 300 K range (between 300 K and 600 K).

Translational kinetic does also depend on the experimental condition and especially on the plasma expansion in the vacuum vessel. For example, Gabriel *et al.* observed, in a cascaded arc[95], kinetic energies higher than 1800 K (8 mm from the source nozzle); Wagner *et al.* measured T_{trans} = 300 K between 500 and 5000 W. Hence our 320 ± 20 K value, both with or without plasma, shows that the plasma expansion in our setup is low, of the same order as a thermal expansion.

5.3. The effect of recombinative desorption on the negative ion production yield

As mentioned in section 1.1 and presented in equation 1, the production of negative ions by dissociative electron attachment (DEA) mechanism is much more efficient when high v″ molecules and electrons of energy below 1 eV interact; similar to DEA, molecular assisted recombination (MAR) needs high v″ for being efficient. For the negative ion production, the effect of metallic surfaces, tantalum in particular, is even more evident when the production rate of DEA (dn_{D^-}/dt) for each v″ level and different materials is evaluated: $n_e \times n_{D_2(v'',J'')} \times k_{DEA}(v'')$. The absolute density of each level ($n_{D_2(v'',J'')}$) is obtained from table VI, the DEA coefficient rate ($k_{DEA}(v'')$) is calculated with the DEA cross section given by Celiberto *et al.*[9] (extrapolated above v″ =6), and the electron energy distribution function (EEDF), bi-maxwellian, is drawn out from previous experiments[51,78] in similar experimental conditions. The result of this coarse evaluation, presented in Fig. 15, emphasizes the surface effect on the negative ion production and the essential role of high vibrationnaly excited levels (the production rate is significant above v″ = 4). At v″ = 7, the tantalum increases, by a factor 3 compared to Quartz (weak surface production of v″) and by a factor 1.3 compared to stainless steel, the production rate. At v″ = 8 and v″ = 9, where Quartz contribution is no longer observed, the tantalum induces an enhancement of the negative ion production rate by a factor 1.3 and 1.9 compared to stainless steel and tungsten, respectively.

If these production rates are summed up for each material, firstly a comparison of their ability to produce negative ions, for a given and identical EEDF of electrons, is possible. Secondly, if the sum of the production rate obtained for stainless steel is correlated to the density of negative ions measured by Kurutz *et al.*[28] for stainless steel this comparison could be made for tantalum and caesium. Hence with this hypothesis, we obtain an absolute density of negative ions of $\sim 1.2 \times 10^{15}\ m^{-3}$ for tantalum which is close to the experimental value obtained by these authors for the same material ($\sim 1.1^{+0.3}_{-0.3} \times 10^{15}\ m^{-3}$) but remains lower than the one obtained with caesium ($> 2.5 \times 10^{15}\ m^{-3}$) in the same plasma conditions (ECR plasma, 300 W,

3×10^{-3} $mbar$). We should note that the density of negative ions obtained by Kurutz *et al.* in ECR laboratory plasma with Cs is lower than the one measured in the ITER-like ion source named BATMAN (RF plasma, 150 kW, 3×10^{-3} $mbar$)[97]: $\sim 10^{17}$ m^{-3}. It is also interesting to compare our results obtained with the bare Quartz surface, which mirrors the volume production with minor contribution of the surface, with the ones by Kurutz *et al.* considering the abovementioned hypothesis. This yields a volume produced negative ion density of $\sim 0.09 \times 10^{15}$ m^{-3}, which is lower than the density given by those authors (0.9×10^{15} m^{-3}, stainless steel).

These measurements also indicate a possibility to increase, in Cs-free plasma, the production rate of negative ions through DEA mechanism: the absolute density of $X\ ^1\sum_g^+(v" = 7) = 4.20 \times 10^{17}$ m^{-3} for a Ta coverage whilst the density of cold electrons is only $\sim 3.50 \times 10^{15}$ m^{-3}. Hence, coverage of the plasma-facing walls with Ta coverage and an increase of the cold electron density could be efficient to improve the density of D^-.

5.4. Conclusions

The direct and accurate measurement of the ro-vibrational population of the D_2 molecule in its electronic ground state was obtained, in an ECR plasma, by the unique combination between synchrotron radiation source and VUV-FTS. The procedures and the operating conditions have allowed a direct comparison of the effect of different materials facing the plasma on the production, through recombinative desorption mechanism, of high v$''$ vibrationnaly excited molecules in the electronic ground state. Tantalum has showed its ability to increase the yield of formation of such high v$''$ molecules (see Figs. 12 and table VI). These unique VUV-FTS measurements also demonstrate the possibility to obtain not only the absolute vibrational distribution function (VDF) of molecules but also their energy distribution over the vibrational, rotational and translational degree of freedom. It also leads to the possibility, not presented in this paper, to obtain the absolute density of D-atoms through the Lyman-series.

A major improvement, for future runs on the DESIRS beamline, will be to reduce the passive gas contribution outside of the plasma core (particularly in the intermediate regions). This will be provided by shortening the distance between the plasma region and the differential pumping regions together with increasing the pumping rate. It will improve in particular the determination of the v$'' = 0$ population in the plasma.

During the same run #20180137 at SOLEIL synchrotron, similar datasets have been obtained for H_2 which will be the subject of a forthcoming paper.

6. ACKNOWLEDGMENTS

This work has been carried out within the framework of the French Federation for Magnetic Fusion Studies (FR-FCM) and of the Eurofusion consortium, and has received funding from the Euratom research and training program 2014-2018 and 2019-2020 under grant agreement No 633053. The views and opinions expressed herein do not necessarily reflect those of the European Commission.

Experiments were performed on the DESIRS beamline at SOLEIL Synchrotron, France, under proposal #20180137. We are grateful to N. de Oliveira and D. Joyeux for his very efficient assistance with the VUV Fourier transform spectrometer, to J.-F. Gil for his technical support for the technical design and for the implementation of our setup in the VUV-FTS beamline, to the beamline manager L. Nahon and to the SOLEIL staff for smoothly running the facility.

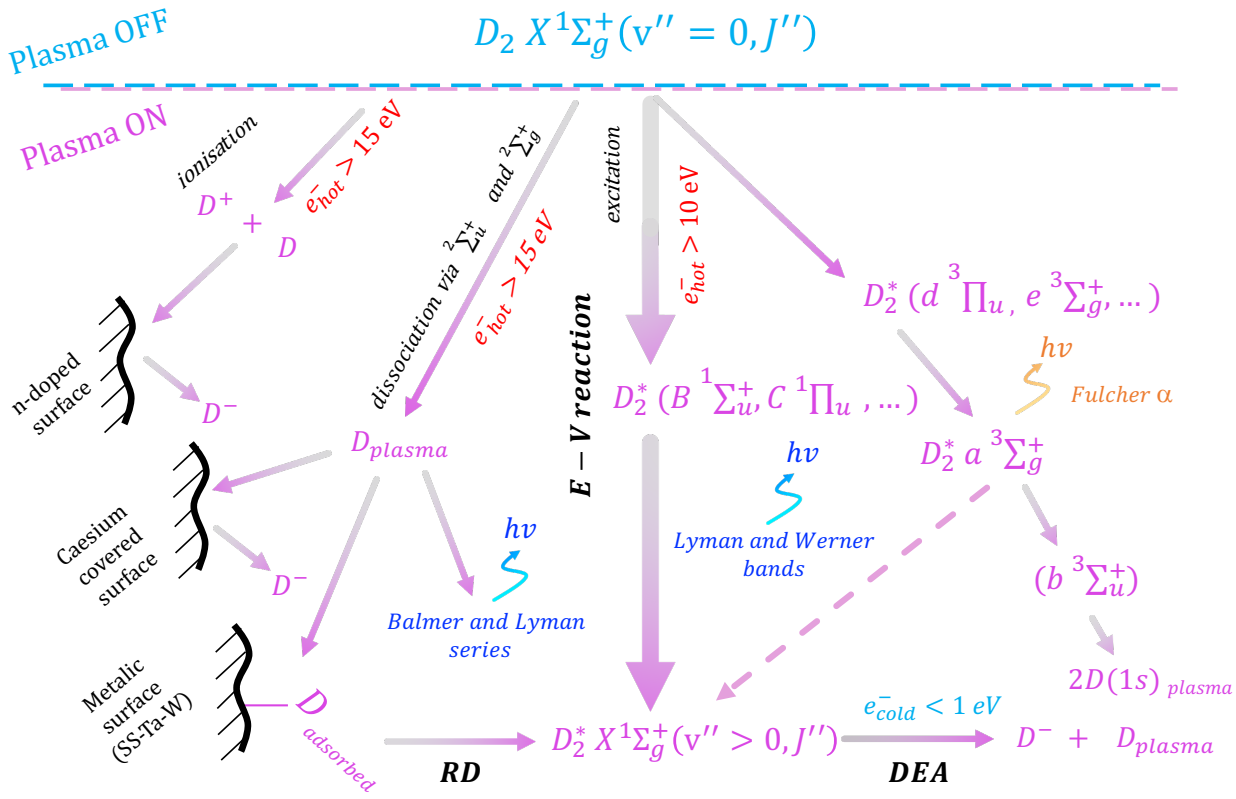

Figure 1: Schematic of the principal routes for the production of $D_2(X^1\sum_g^+, v")$ molecules.

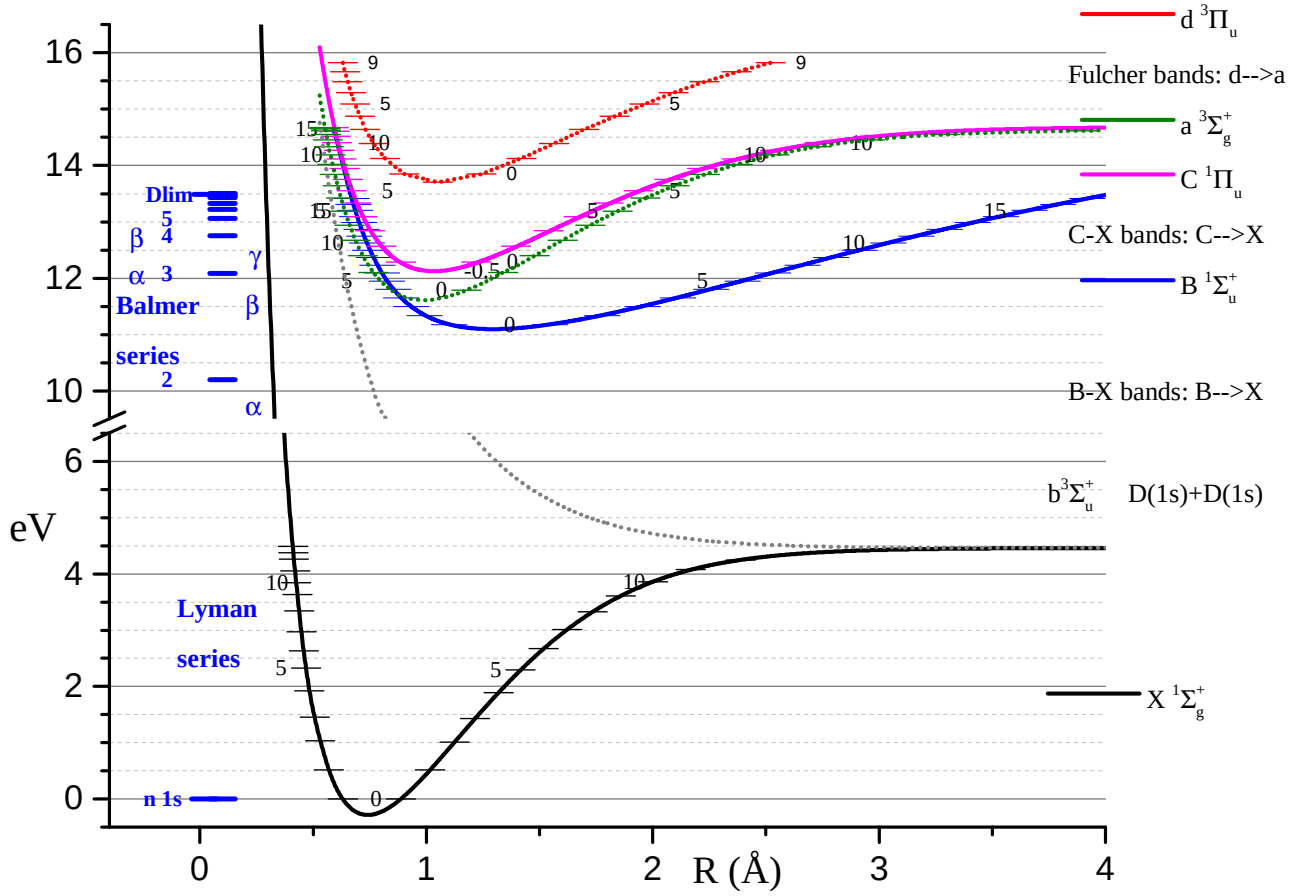

Figure 2: Energy diagram for D_2 and D (3 eV break in the energy scale).

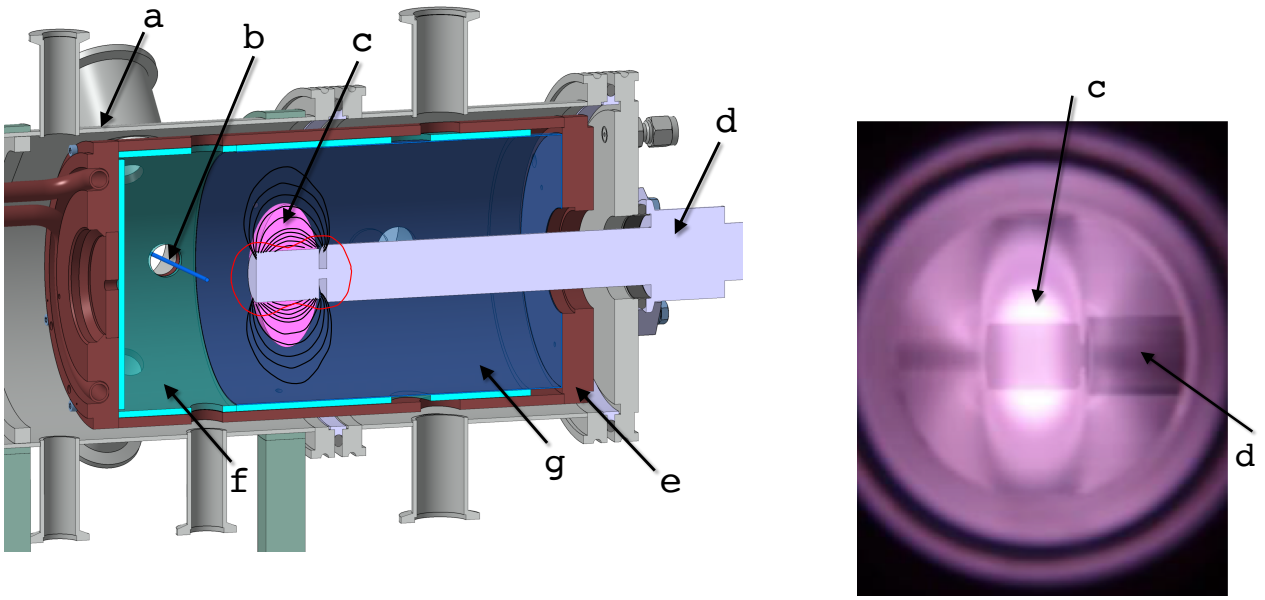

(a) **(b)**

Figure 3: Schematic of the SCHEMEII+ experimental setup, 3a). The plasma source, d, is plugged to the reactor. The plasma produced around the magnet of the plasma source (pink area, c) expands in a Quartz cylinder, f, housed in a cooled-copper cylinder, e, and all sets inside the reactor stainless steel cylinder, a. The foil of the sample material, g, is placed on the inner surface of the Quartz cylinder. The main pumping unit, not represented on the schematic, is set on the left side of the reactor. The synchrotron beam light is represented by a blue line, b, throughout a viewport on the left. Close to the plasma source magnet, magnetic field lines are represented in black and intensity of 0.0875 T is highlighted by a red line. 3b), Picture of an ECR plasma source, d, in functioning. The ECR coupling zone, close to the encapsulated permanent magnet, appears as the white glowing zone, c.

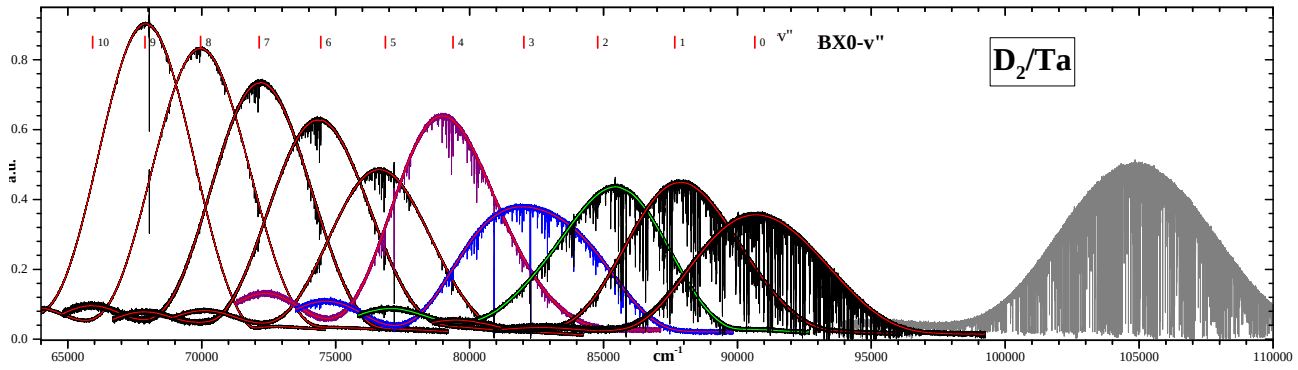

Figure 4: Raw spectra given by the VUV-FTS for ten undulator settings in the 64000-96000 cm^{-1} energy range from BX09 (to the left) to BX00 and an additional range 100000-111000 cm^{-1} for the D Lyman series (to the right).

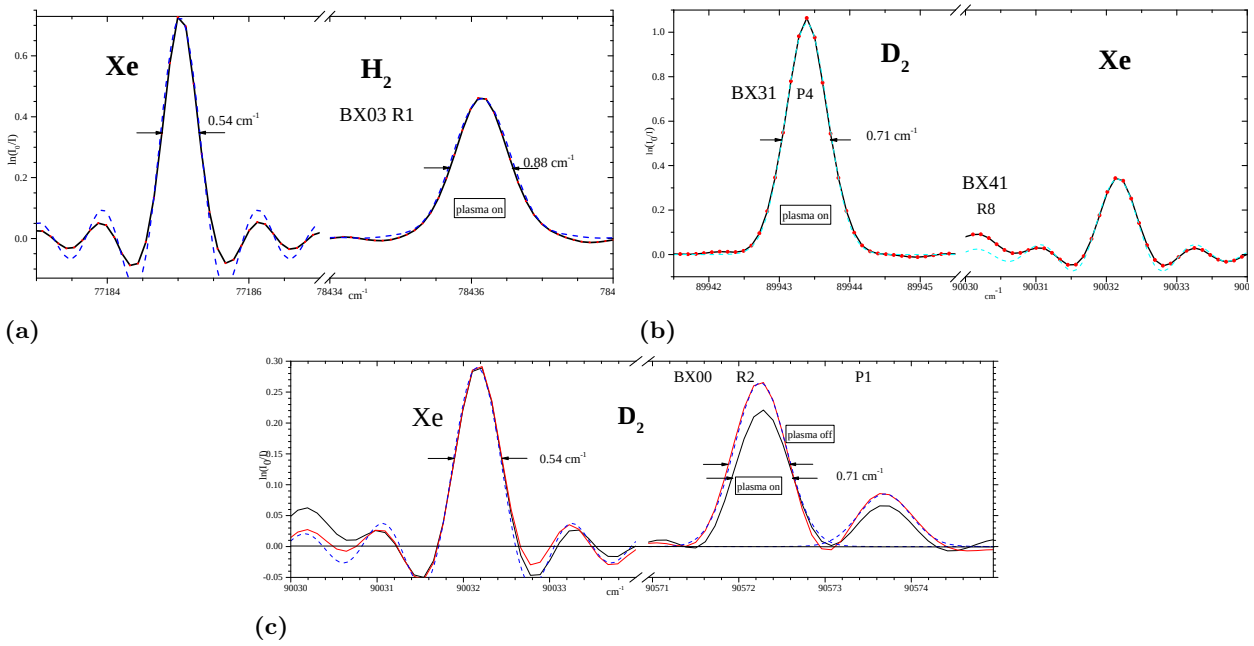

Figure 5: Comparison between Xe, H_2 and D_2 lines. (Figs. 5a, 5b): with plasma, H_2 BX03 R1 and D_2 BX31 P4. (Fig. 5c) D_2 BX00 R2 and P1 lines, plasma OFF in red and plasma ON in black. All molecular lines are adjusted by a sinc-convoluted Gaussian function; in each sub-figure the scale ranges are the same: 4 cm^{-1}.

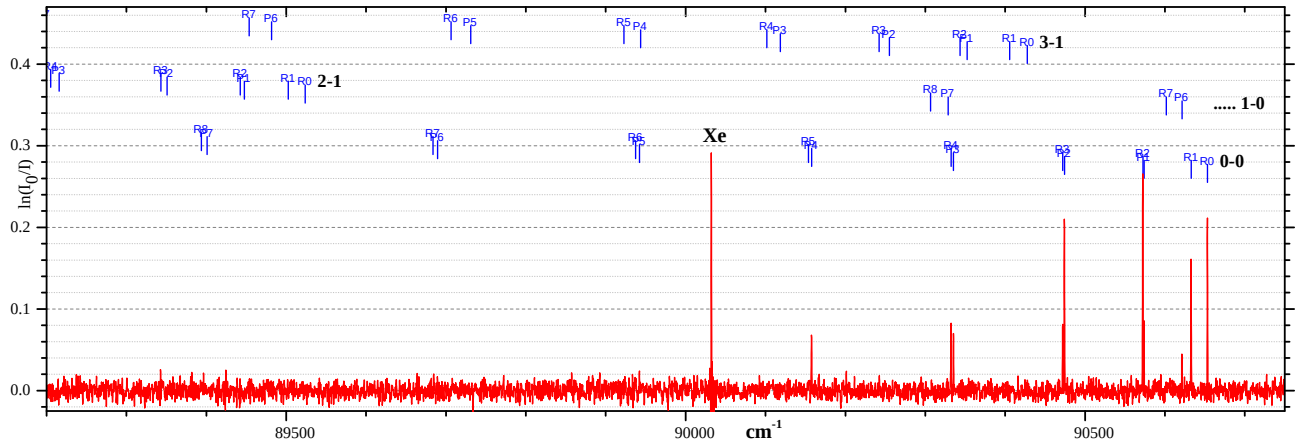

(a) Plasma OFF

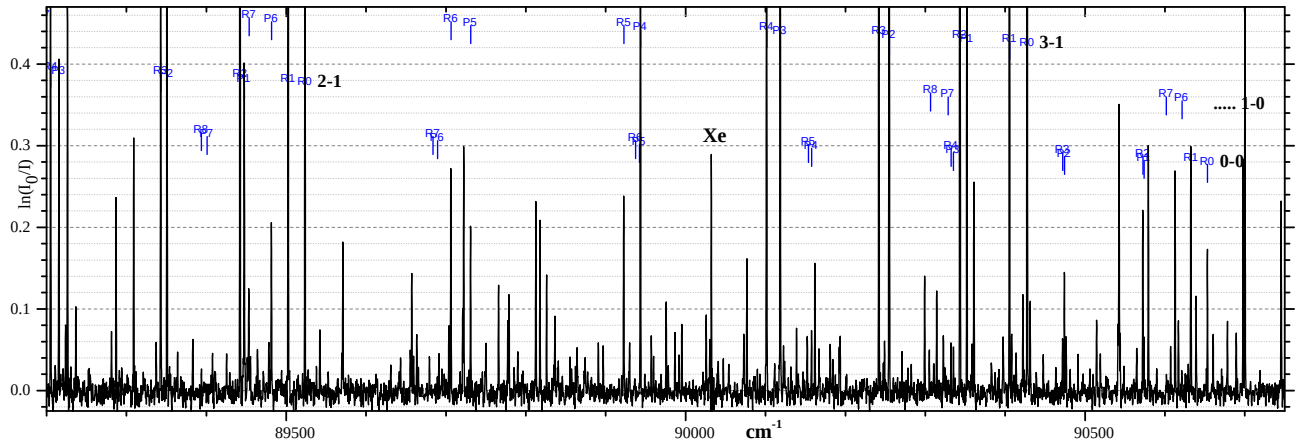

(b) Plasma ON

Figure 6: BX00 band absorption spectrum 6a: without plasma and 6b: with plasma (plasma conditions: 8 μbar, 150 W).

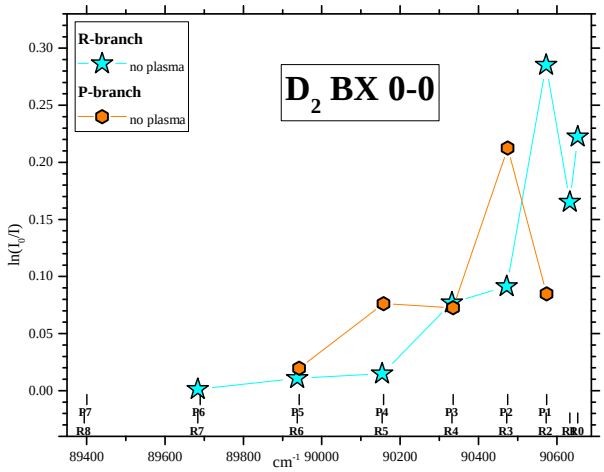

(a) Plasma OFF

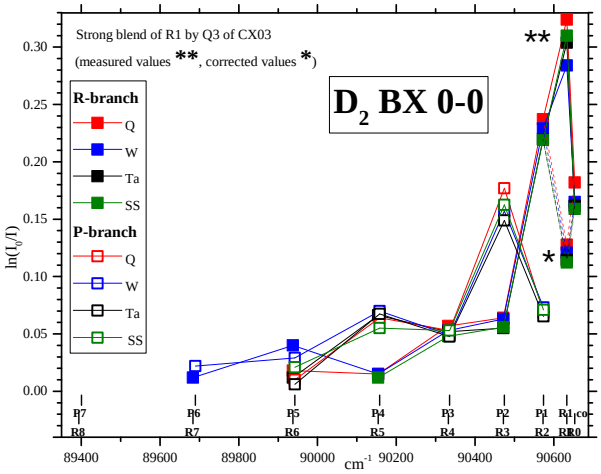

(b) Plasma ON

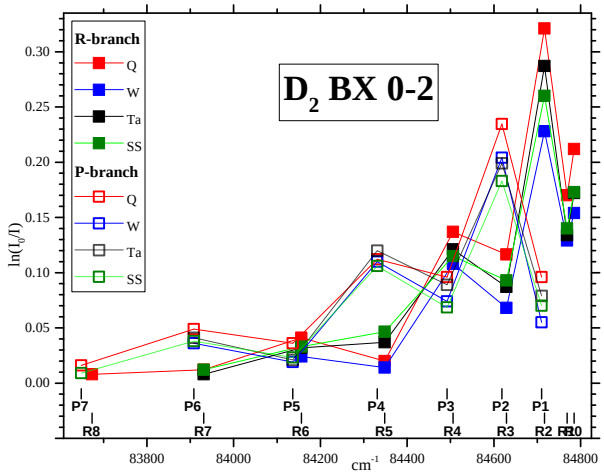

(c) Plasma ON

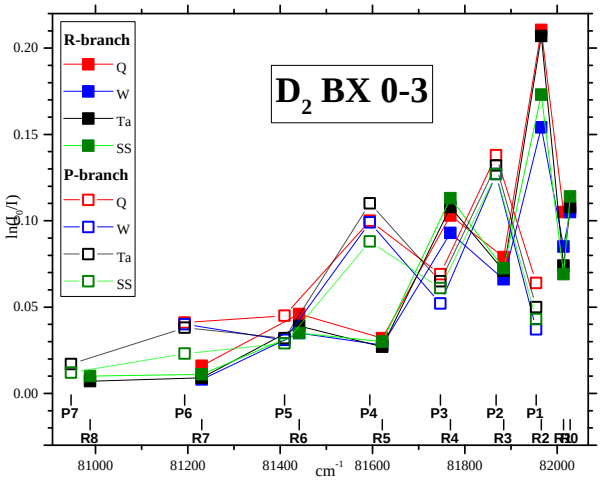

(d) Plasma ON

Figure 7: Samples of line optical depths for the R- and P-branches versus the corresponding transition energies for the BXv′0 transitions; (7a) BX00 without plasma and (7b) BX00 with plasma and showing the measured and corrected values for R1, (7c) BX02 and (7d) BX03.

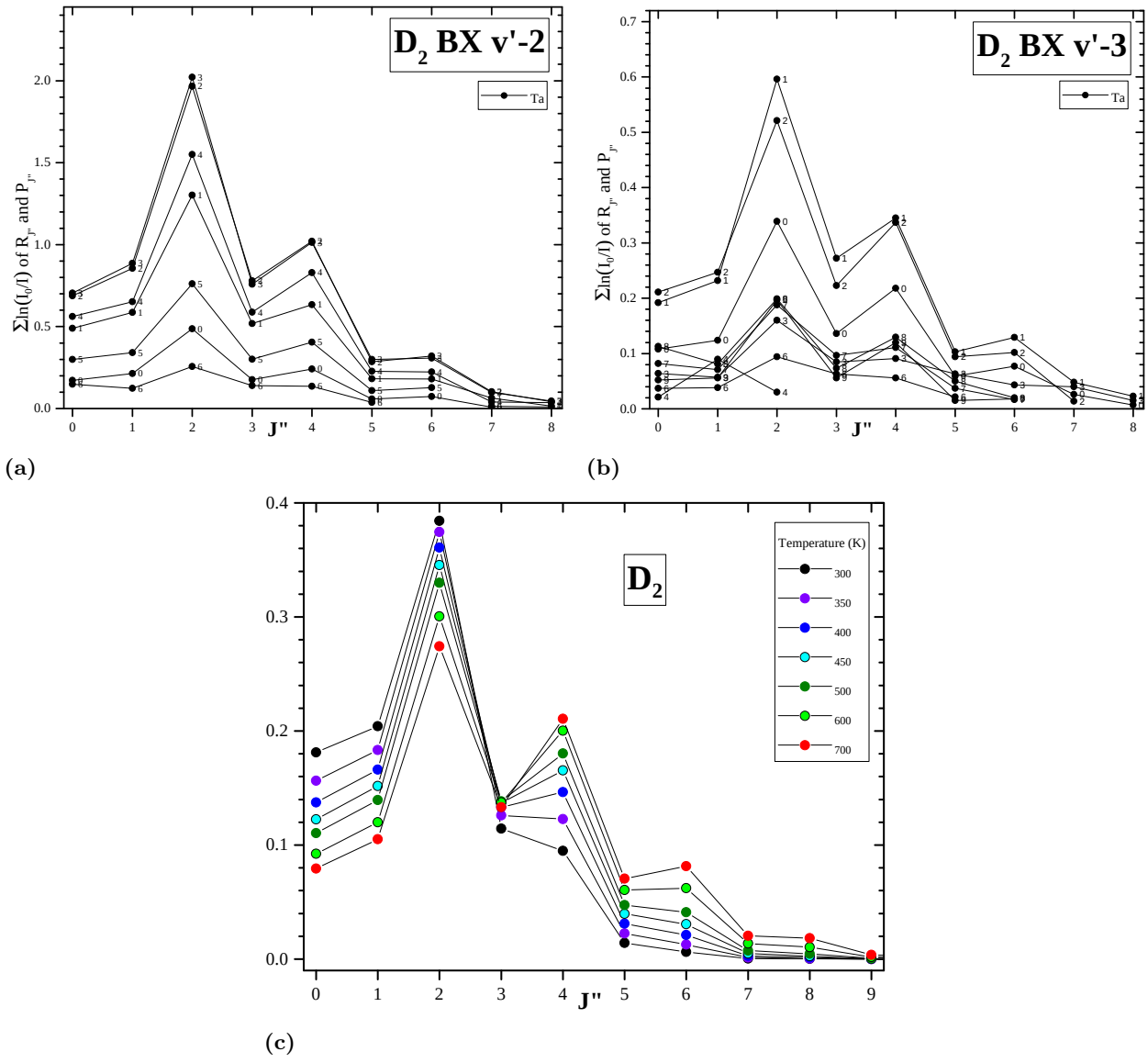

Figure 8: Samples of the sum of the optical depths for $R_{J''}$ and $P_{J''}$ versus J'' for the BXv'-v''transitions (here $v'' = 2$ and 3, in Figs. 8a and 8b, respectively) in the case of tantalum wall material. In each figure, curves are labelled with v'. Fig.8c rotational distribution function computed for several temperatures (between 300 and 700 K) in the case of pure Boltzmann distributions

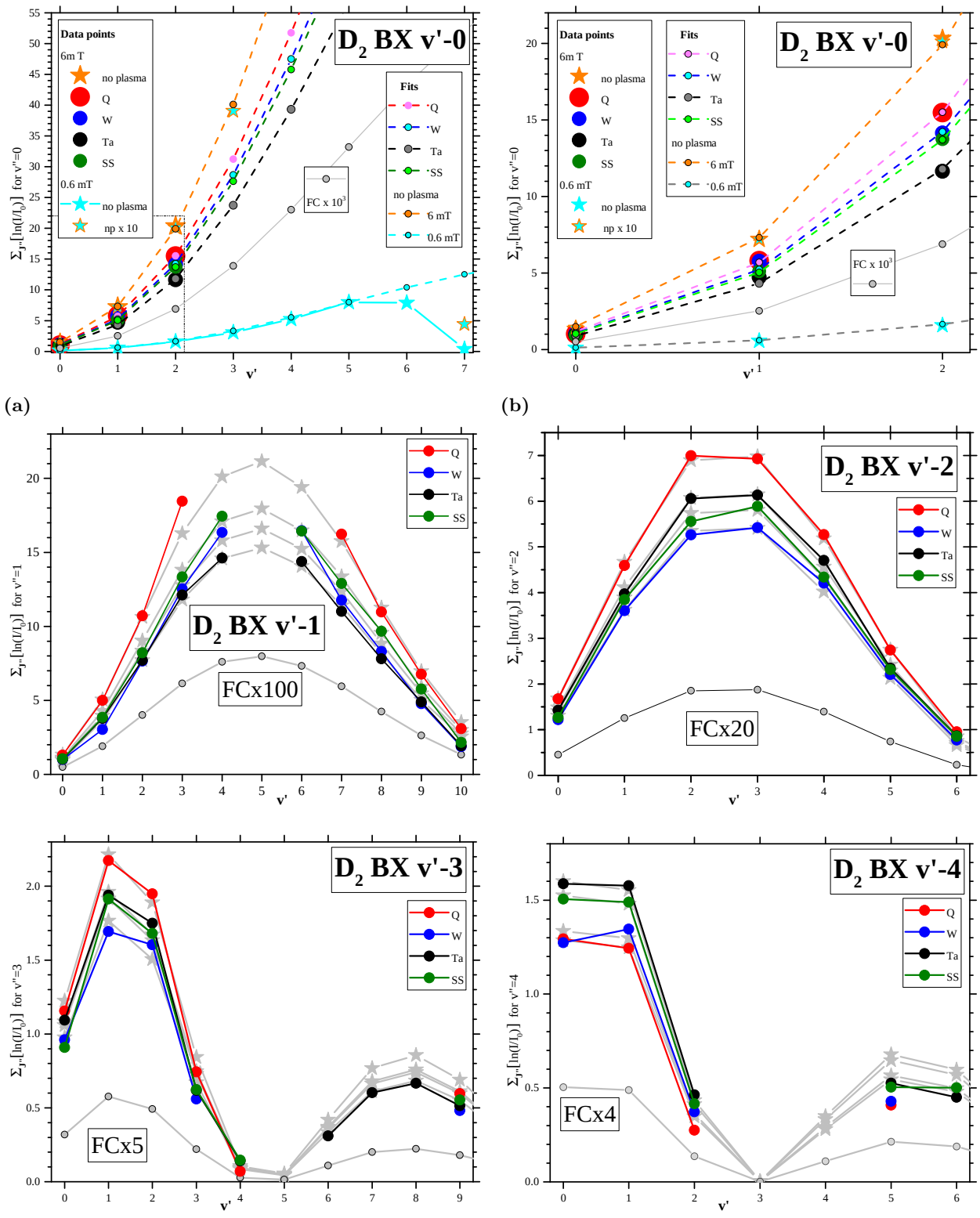

Figure 9: Each figure shows for a vibrational level v'' the sum of the corresponding J'' optical depths versus v' . These numbers are proportional to the total populations in the v'' vibrational ground levels of D_2. The missing data points for $BX v'0$ and $BX v'1$ (9a) correspond to strongly absorbed transitions. The second figure for for $BX v'0$ (9b) is a zoom for low v' (0, 1 and 2) of the first one. The fits performed for each wall material are traced in gray color stars underneath our data points and the tabulated FC times different factors are also indicated with small black circle.

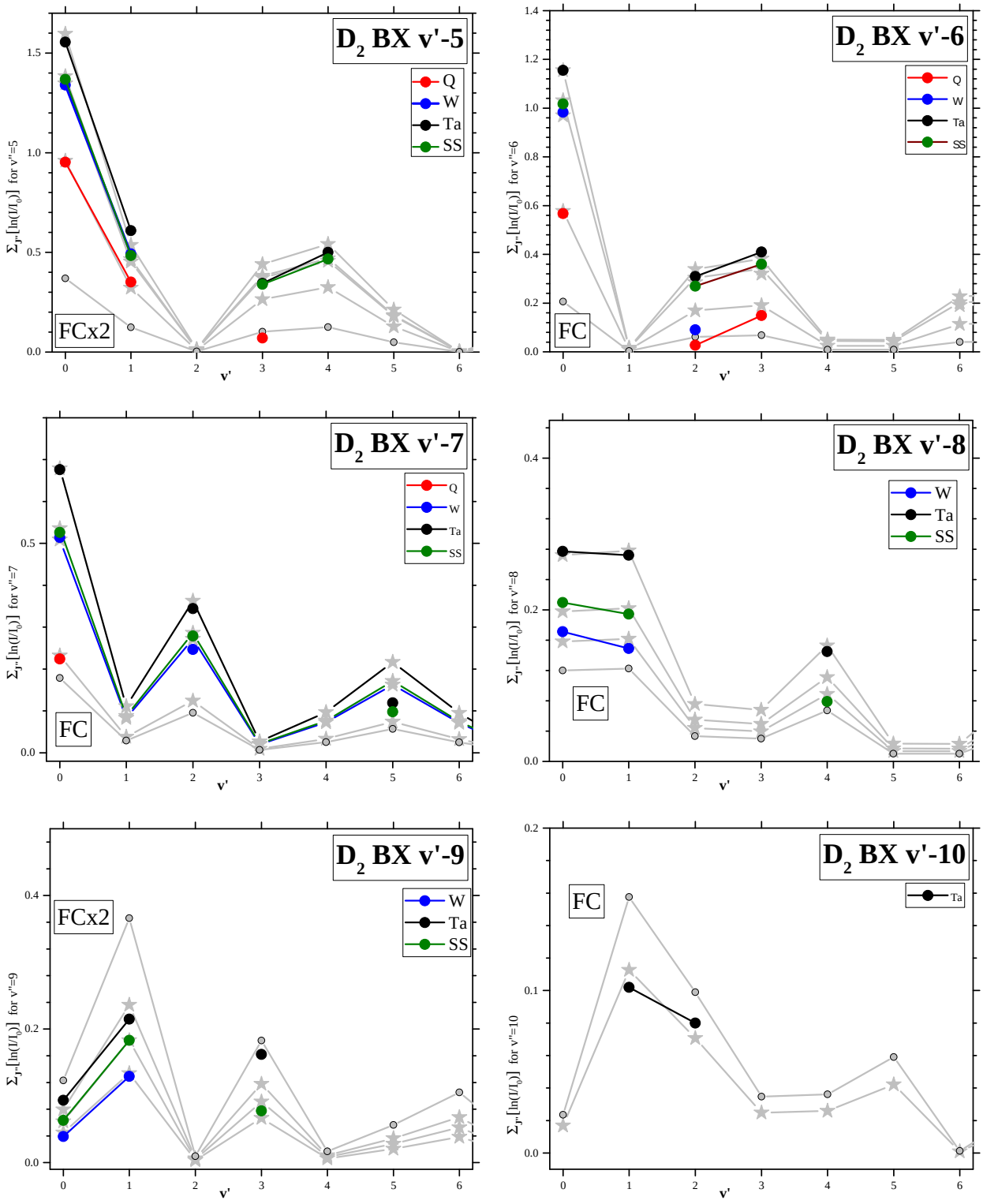

Figure 9: Continued.

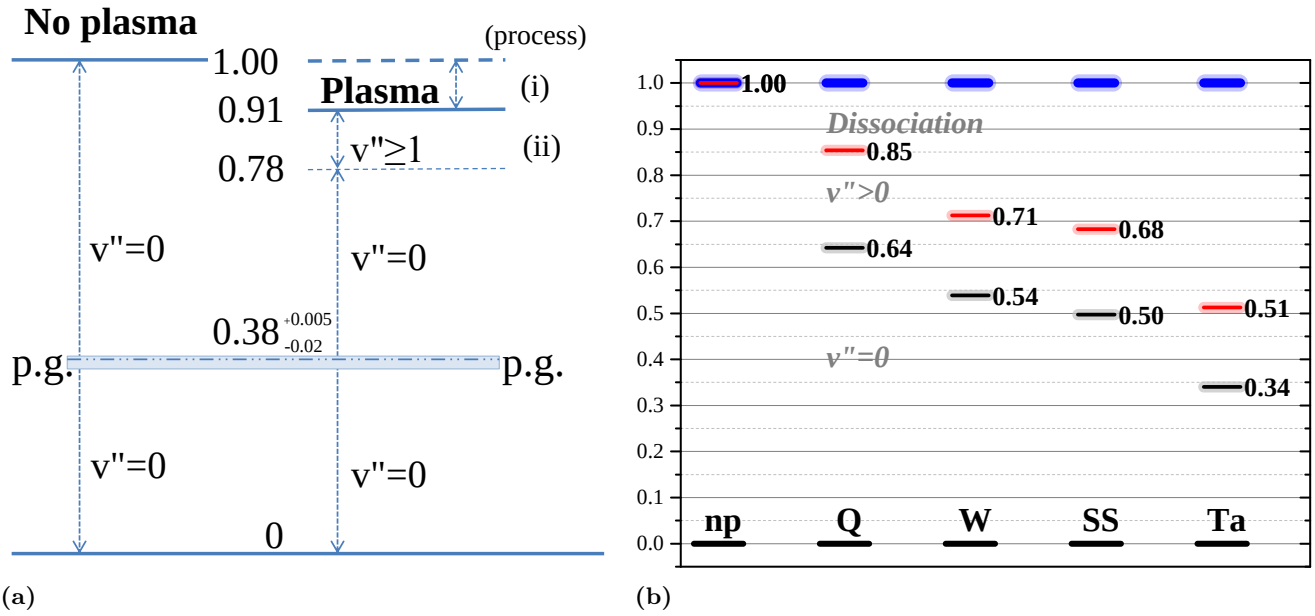

Figure 10: Scheme of the D_2 vibrational population distribution in the X $^1\Sigma_g^+$ ground state without and with plasma excitation (150 W, 8 µbar). Fig.10a: The total measured signal including the passive gas (p.g.) with its error bar is given for the Quartz surface; Fig.10b: after p.g. subtraction on the four materials. Both graphs are normalized to unity. See texts in the last paragraph of section 3 and in section 4.1 for details.

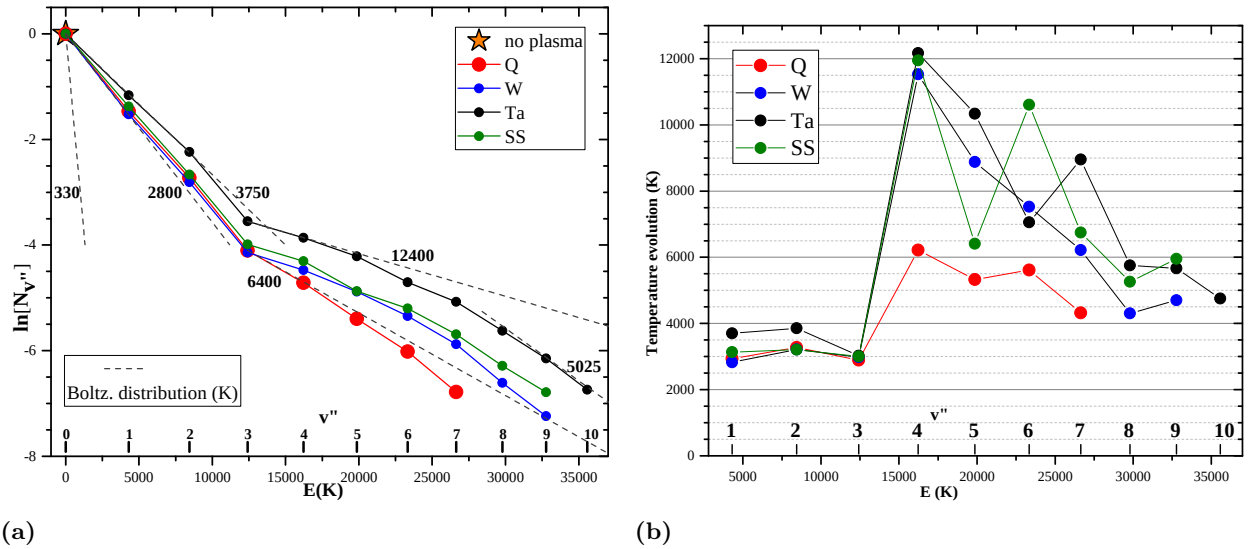

Figure 11: D_2 relative vibrational v'' level populations (normalized to $v'' = 0$ w/o plasma) for the four material studied: Q, W, Ta and SS (for more clarity, the curves for the 3 metals are shifted up to zero for $v'' = 0$). Fig. 11a. Temperature evolution between two adjacent v'', Fig. 11b

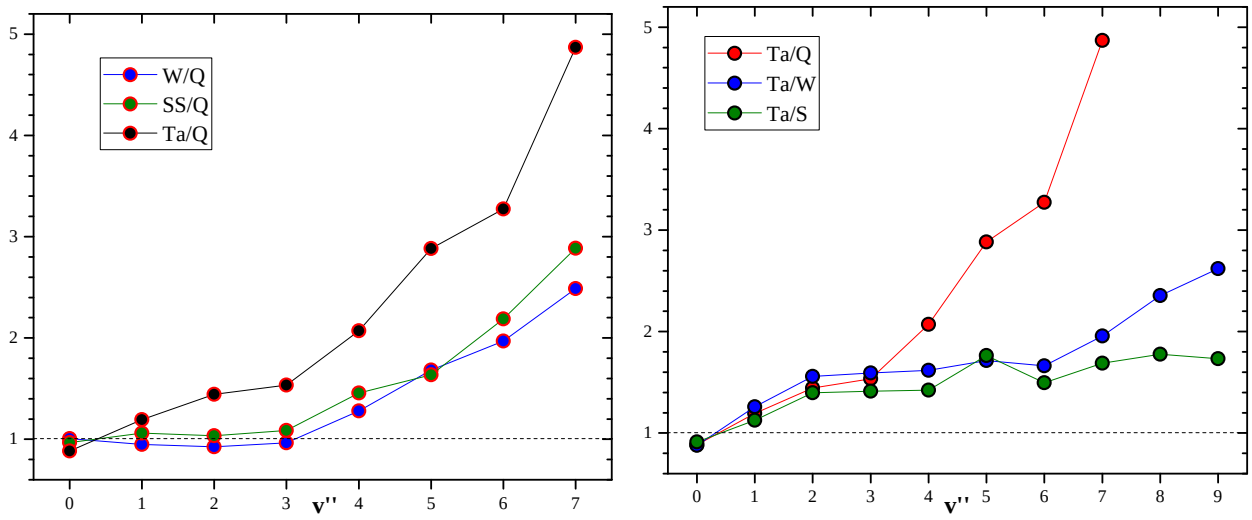

(a) (b)

Figure 12: a) Recombinative desorption rate of W, Ta and SS compared to Quartz vs. v''. b) comparison of Q, W and SS to Tantalum vs. v''.

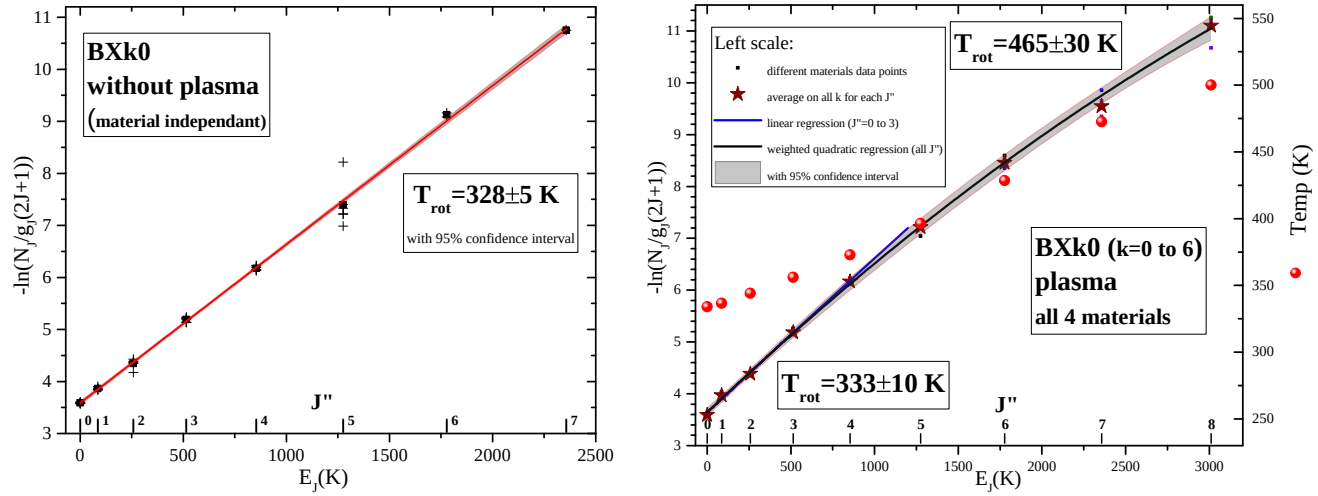

(a) (b)

Figure 13: D_2 Boltzman plot derived rotational temperatures. Fig.13a: without plasma, from BXk0 ($k = 0$ to 5) measurements at 8 and 0.8 μbar (38 data points), Fig.13b: with plasma excitation at 150 W, 8 μbar and averaged on all wall materials, from BXk0 ($k = 0$ to 6) measurements at 8 μbar (128 data points). On the right scale, the approximate rotational temperature is derived from the second order fit. All linear regressions for low J'' are weighted by the number of data points per J''.

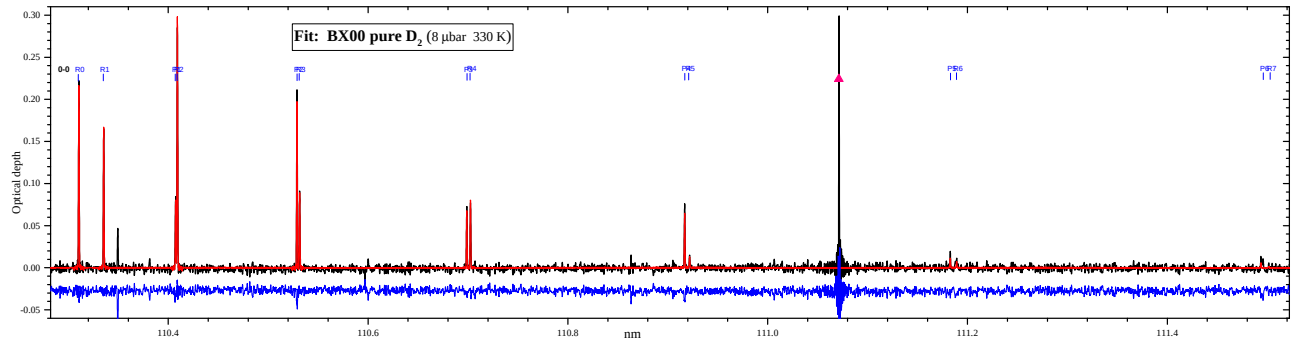

(a)

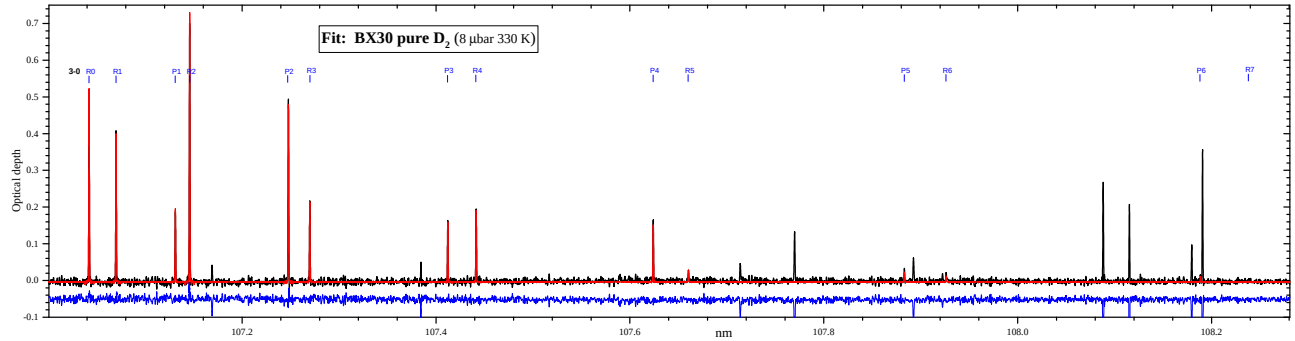

(b)

Figure 14: Fits of the BX00 (8 µbar, Fig. 14a) and BX30 (0.8 µbar, Fig. 14b) rotational spectra at 330 K. Recorded spectrum (black), fit (red) and residual (blue). A Xe I line is lying at 111.07 nm and a few from other D_2 bands are present.

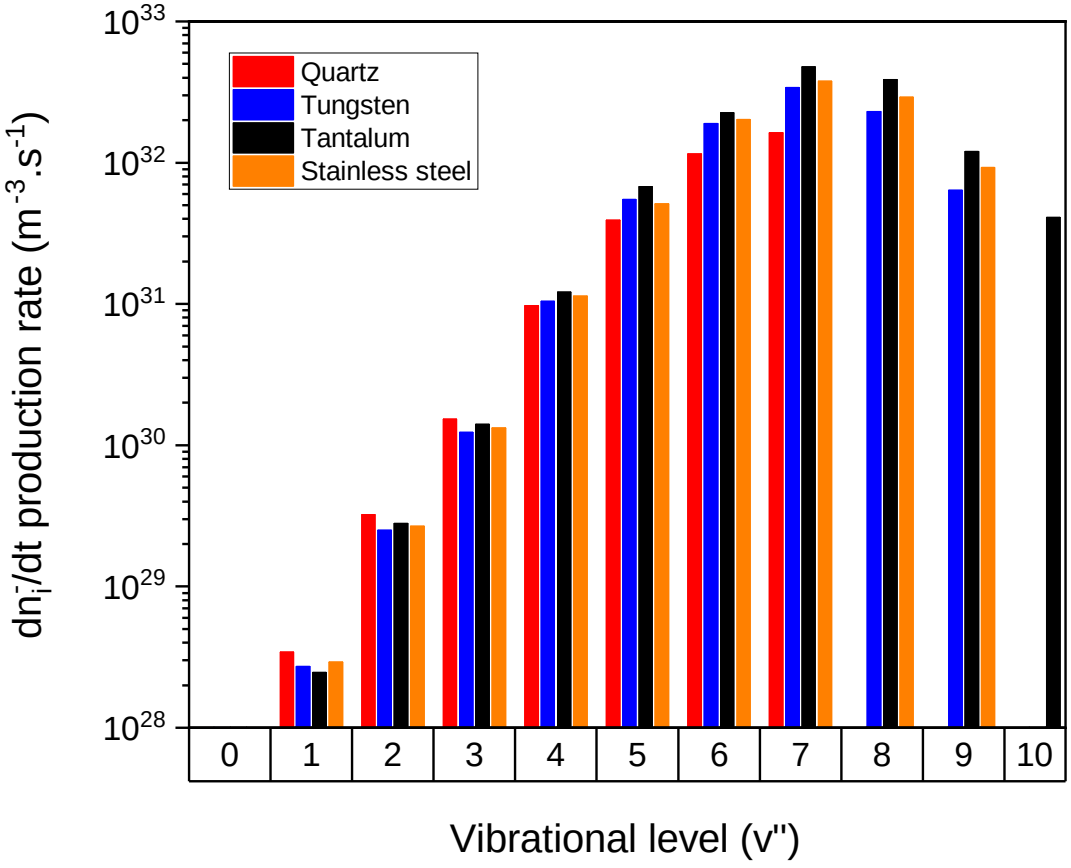

Figure 15: Absolute production yield of negative ions through DEA mechanism for the investigated materials for each quantum level. A theoretical bi-maxwelian EEDF of Te_{cold} *= 1.54 eV and* ne_{cold}*=*$3.9\times10^{15}m^{-3}$ *and* Te_{hot} *= 15.2 eV and* ne_{cold}*=*$2.1\times10^{14}m^{-3}$

are from[78], v″ absolute densities are obtained from Table VI and reaction rate of DEA for each v″ level are from[9].

Acronym	Process	Ref.
Volume reactions		
V-T	$D_2(X^1\sum_g^+, v) + D_2(X^1\sum_g^+, w) \rightarrow D_2(X^1\sum_g^+, v \pm 1) + D_2(X^1\sum_g^+, w)$	98
V-t	$D_2(X^1\sum_g^+, v") + D \rightarrow D_2(X^1\sum_g^+, v') + D$	99
e-V	$D_2(X^1\sum_g^+, v") + e_{hot} \rightarrow D_2(X^1\sum_g^+, v') + e_{cold}$	100,101
E-V	$D_2(X^1\sum_g^+, v') + e_{hot} \rightarrow D_2^*(B^1\sum_u, C^1\prod_u ...) + e_{cold} \rightarrow D_2(X^1\sum_g^+, v") + e_{cold} + h\nu$	102
Surface reactions		
Auger	$D_2^+ + (e)_{surface} \rightarrow D_2(X^1\sum_g^+, v")$	103
Recombinative Desorp.	$D + D_{surface} \rightarrow D_2(X^1\sum_g^+, v")$	50,104

Table I: Principal kinetic processes of $D_2(X^1\sum_g^+, v")$ formation.

BXv'v"	v"											Sum
v'	0	1	2	3	4	5	6	7	8	9	10	
0	✓	✓	✓	✓	✓	✓	✓	✓	✓	✓		10
1	✓	✓	✓	✓	✓	✓			✓	✓	✓	9
2	✓[a]	✓[a]	✓	✓	✓		✓	✓			✓	8
3	✓[a]	✓[a]	✓	✓		✓	✓			✓		7
4	✓[a]	✓[a]	✓	✓		✓			✓			6
5	✓[a]	✓[a]	✓		✓			✓				5
6	✓[a]	✓[a]	✓	✓	✓							5
7	✓	✓[a]		✓								3
8	Nor	✓[a]		✓								2
9	Nor	✓		✓								2
10	Nor	✓										1
Sum	8	11	7	9	5	4	3	3	3	3	2	**58**

[a] Partially saturated bands (optical depth>1.5) at 8 μbar (BXv′0 not saturated at 0.8 μbar)
The checkmark ✓indicates the observed bands while Nor stands for Not in the recorded frequency ranges.

Table II: Recorded bands for D_2 $B^1\Sigma_u^+ - X^1\Sigma_g^+$ transitions.

BXv'v"	v"										
v'	0	1	2	3	4	5	6	7	8	9	10
0	90653.33	87659.71	84785.21	82027.73	79385.62	76857.68	74443.22	72142.07	69954.63	67881.97	65925.88
1	91595.01	88601.39	85726.89	82969.41	80327.3	77799.36	75384.9	73083.75	70896.31	68823.65	66867.56
2	92517.28	89523.66	86649.16	83891.68	81249.57	78721.63	76307.17	74006.02	71818.58	69745.92	67789.83
3	93421.36	90427.74	87553.24	84795.76	82153.65	79625.71	77211.25	74910.1	72722.66	70650	68693.91
4	94307.94	91314.32	88439.82	85682.34	83040.23	80512.29	78097.83	75796.68	73609.24	71536.58	69580.49
5	95177.43	92183.81	89309.31	86551.83	83909.72	81381.78	78967.32	76666.17	74478.73	72406.07	70449.98
6	96030.17	93036.55	90162.05	87404.57	84762.46	82234.52	79820.06	77518.91	75331.47	73258.81	71302.72
7	96866.37	93872.75	90998.25	88240.77	85598.66	83070.72	80656.26	78355.11	76167.67	74095.01	72138.92
8	97686.21	94692.59	91818.09	89060.61	86418.5	83890.56	81476.1	79174.95	76987.51	74914.85	72958.76
9	98489.88	95496.26	92621.76	89864.28	87222.17	84694.23	82279.77	79978.62	77791.18	75718.52	73762.43
10	99277.54	96283.92	93409.42	90651.94	88009.83	85481.89	83067.43	80766.28	78578.84	76506.18	74550.09

Table III: R0 bandhead wavenumbers (cm^{-1}) for D_2 $B^1\Sigma_u^+ - X^1\Sigma_g^+$ transitions.

BXv'v"	v"										
v'	0	1	2	3	4	5	6	7	8	9	10
0	0.0005	0.0050	0.0226	0.0638	0.1260	0.1845	0.2063	0.1786	0.1199	0.0616	0.0236
1	0.0025	0.0190	0.0627	0.1154	0.1224	0.0620	0.0030	0.0292	0.1225	0.1831	0.1575
2	0.0069	0.0401	0.0926	0.0984	0.0342	0.0017	0.0606	0.0955	0.0334	0.0048	0.0990
3	0.0139	0.0615	0.0937	0.0439	0.0002	0.0510	0.0681	0.0070	0.0300	0.0915	0.0347
4	0.0230	0.0760	0.0696	0.0055	0.0275	0.0626	0.0089	0.0255	0.0673	0.0084	0.0361
5	0.0332	0.0798	0.0369	0.0028	0.0534	0.0246	0.0088	0.0570	0.0103	0.0282	0.0590
6	0.0433	0.0733	0.0114	0.0218	0.0470	0.0003	0.0406	0.0250	0.0102	0.0526	0.0013
7	0.0522	0.0594	0.0005	0.0400	0.0220	0.0108	0.0424	0.0001	0.0420	0.0121	0.0267
8	0.0590	0.0425	0.0029	0.0446	0.0031	0.0314	0.0178	0.0147	0.0331	0.0035	0.0426
9	0.0635	0.0263	0.0130	0.0360	0.0012	0.0377	0.0008	0.0341	0.0060	0.0287	0.0123
10	0.0655	0.0133	0.0244	0.0212	0.0116	0.0271	0.0050	0.0309	0.0019	0.0333	0.0010

Table IV: Franck-Condon factors for D_2 $B^1\Sigma_u^+ - X^1\Sigma_g^+$ transitions[32].

v''	D_2 w/o plasma	D_2 /Q	D_2 /W	D_2 /SS	D_2 /Ta
0	1.0E+00	7.8E-01	7.1E-01	6.9E-01	5.9E-01
1		9.2E-02	7.3E-02	7.8E-02	6.6E-02
2		2.6E-02	2.0E-02	2.1E-02	2.2E-02
3		6.6E-03	5.3E-03	5.7E-03	6.1E-03
4		3.6E-03	3.8E-03	4.2E-03	4.4E-03
5		1.8E-03	2.5E-03	2.4E-03	3.1E-03
6		9.7E-04	1.6E-03	1.7E-03	1.9E-03
7		4.5E-04	9.3E-04	1.0E-03	1.3E-03
8			4.5E-04	5.7E-04	7.6E-04
9			2.4E-04	3.5E-04	4.5E-04
10					2.5E-04
Σ v'' >0		1.3E-01	1.1E-01	1.2E-01	1.1E-01
Σ v''	1.0E+00	9.1E-01	8.2E-01	8.0E-01	7.0E-01
Unaccounted-for		9.0E-02	1.8E-01	2.0E-01	3.0E-01
Checksum	1.0E+00	1.0E+00	1.0E+00	1.0E+00	1.0E+00

Table V: D_2 normalized total populations in the v'' vibrational levels of the $X^1\Sigma_g^+$ ground state. These data correspond to average values along the total path where D_2 is present, i.e. the plasma core and the passive gas in the two differential pumping regions at both sides of the reactor. Col. 2: pure gas without plasma; cols. 3 to 6: with Quartz, Stainless Steel, Tungsten, and Tantalum wall material (plasma conditions: 8 μbar, 150 W excitation). The penultimate line gives the total population of molecules which are dissociated, ionized, or excited in triplet states, consequently not accounted.

v''	D_2 w/o plasma	D_2 /Q	D_2 /W	D_2 /SS	D_2 /Ta
0	1.98E+14	1.27E+14	1.07E+14	9.83E+13	6.73E+13
1		2.93E+13	2.32E+13	2.49E+13	2.10E+13
2		8.29E+12	6.41E+12	6.86E+12	7.19E+12
3		2.10E+12	1.69E+12	1.82E+12	1.93E+12
4		1.14E+12	1.22E+12	1.33E+12	1.42E+12
5		5.75E+11	8.07E+11	7.52E+11	9.95E+11
6		3.10E+11	5.09E+11	5.42E+11	6.08E+11
7		1.44E+11	2.99E+11	3.32E+11	4.20E+11
8			1.44E+11	1.82E+11	2.43E+11
9			7.63E+10	1.11E+11	1.44E+11
10					7.96E+10
v'' >0		4.19E+13	3.44E+13	3.68E+13	3.40E+13
Σ v''	1.98E+14	1.69E+14	1.41E+14	1.35E+14	1.01E+14
Unaccounted-for		2.89E+13	5.68E+13	6.27E+13	9.64E+13
Checksum	1.98E+14	1.98E+14	1.98E+14	1.98E+14	1.98E+14
Σv'' >0/Σv''		24.8	24.4	27.2	33.6
Σv'' >0/v'' = 0		33.0	32.3	37.4	50.6
Dissoc./ Σv''		17.1	40.3	46.4	95.1

*Table VI: D_2 absolute molecular densities (cm^{-3}) in the plasma core region, in the v'' vibrational levels of the $X^1\Sigma_g^+$ electronic ground state, the sum in all excited v''>0 levels, the sum in all v'' levels [process (**ii**)], and the molecules which are which are dissociated, ionized, or excited in triplet states, consequently not accounted. [process (**i**)] (see last paragraph of 4.1). Two times this last value corresponds to the atomic deuterium absolute density in the plasma. The three last lines give the percentages of molecules in a v''>0 level compared to Σv'' and v'' = 0 and the number of dissociated ones compared to Σ v''. A gas temperature of 293 K is considered without and with plasma.*

REFERENCES

[1] M. Agundez, J. R. Goicoeche, J. Cernicharo, A. Faure, and E. Roueff, "The chemistry of vibrationally excited H2 in the interstellar medium," Astron. J., vol. 713, no. 1, 2010.

[2] W. W. Duley and D. A. Williams, "The formation of H2 on interstellar dust," Mon. Not. R. Astron. Soc., vol. 260, pp. 37–42, jan 1993.

[3] J. M. Shull and S. Beckwith, "Interstellar Molecular Hydrogen," Annu. Rev. Astron. Astrophys., vol. 20, pp. 163–190, sep 1982.

[4] K. Sawada and T. Fujimoto, "Effect of Initial Vibrational Excitation of Molecular Hydrogen on Molecular Assisted Recombination in Divertor Plasmas," Contrib. to Plasma Phys., vol. 42, pp. 603–607, nov 2002.

[5] S. I. Krasheninnikov, "Molecule Assisted Recombination (MAR): Mechanisms and Plasma Conditions for Effective Operation," Phys. Scr., vol. T96, no. 1, p. 7, 2002.

[6] M. Allan and S. F. Wong, "Effect of Vibrational and Rotational Exictation on Dissociative Attachment in Hydrogen," Phys. Rev. Lett., vol. 41, pp. 1791–1794, dec 1978.

[7] R. Celiberto, R. Janev, J. Wadehra, and J. Tennyson, "Dissociative electron attachment to vibrationally excited H2 molecules involving the 2Σg+ resonant Rydberg electronic state," Chem. Phys., vol. 398, pp. 206–213, apr 2012.

[8] C. Gorse, R. Celiberto, M. Cacciatore, A. Laganá, and M. Capitelli, "From dynamics to modeling of plasma complex systems: negative ion (H-) sources," Chem. Phys., vol. 161, pp. 211–227, apr 1992.

[9] R. Celiberto, R. K. Janev, A. Laricchiuta, M. Capitelli, J. M. Wadehra, and D. E. Atems, "Cross section data for electron-impact inelastic processes of vibrationally excited molecules of hydrogen and its isotopes," At. Data Nucl. Data Tables, vol. 77, pp. 161–213, mar 2001.

[10] H. Abe, M. Yoneda, and N. Fujiwara, "Developments of Plasma Etching Technology for Fabricating Semiconductor Devices," Jpn. J. Appl. Phys., vol. 47, pp. 1435–1455, mar 2008.

[11] E. Krishnakumar and K. Nagesha, "Dissociative attachment studies by negative-ion time-of-flight mass spectrometry," Rapid Commun. Mass Spectrom., vol. 9, pp. 336–343, jan 1995.

[12] J. G. Dillard, "Negative ion mass spectrometry," Chem. Rev., vol. 73, pp. 589–643, dec 1973.

[13] N. Hershkowitz, "Role of plasma-aided manufacturing in semiconductor fabrication," IEEE Trans. Plasma Sci., vol. 26, no. 6, pp. 1610–1620, 1998.

[14] G. I. Dimov, "Use of hydrogen negative ions in particle accelerators," Rev. Sci. Instrum., vol. 67, no. 10, pp. 3393–3404, 1996.

[15] D. P. Moehs, J. Peters, and J. Sherman, "Negative hydrogen ion sources for accelerators," IEEE Trans. Plasma Sci., vol. 33, no. 6, pp. 1786–1798, 2005.

[16] J. Peters, "Negative ion sources for high energy accelerators (invited)," Rev. Sci. Instrum., vol. 71, pp. 1069–1074, feb 2000.

[17] B. Goddard, W. Bartmann, M. Benedikt, T. Kramer, and A. Koschik, "4 GeV H- Charge Exchange Injection into the PS2," in EPAC 08, 11th Eur. Partcle Accel. Conf., (Geneva, Switzerland), CERN-AB-2008, sep 2008.

[18] M. Bacal and M. Wada, "Negative ion source operation with deuterium," Plasma Sources Sci. Technol., vol. 29, p. 033001, mar 2020.

[19] R. S. Hemsworth, D. Boilson, P. Blatchford, M. D. Palma, G. Chitarin, H. P. De Esch, F. Geli, M. Dremel, J. Graceffa, D. Marcuzzi, G. Serianni, D. Shah, M. Singh, M. Urbani, and P. Zaccaria, "Overview of the design of the ITER heating neutral beam injectors," 2017.

[20] M. Kikuchi, K. Lackner, M. Q. Tran, and International Atomic Energy Agency., Fusion physics. International Atomic Energy Agency, 2012.

[21] P. Agostinetti, T. Franke, U. Fantz, C. Hopf, N. Mantel, and M. Q. Tran, "RAMI evaluation of the beam source for the DEMO neutral beam injectors," Fusion Eng. Des., vol. 159, p. 111628, oct 2020.

[22] U. Fantz, R. Gutser, and C. Wimmer, "Fundamental experiments on evaporation of cesium in ion sources," Rev. Sci. Instrum., vol. 81, no. 2, p. 02B102, 2010.

[23] M. Bacal and M. Wada, "Negative hydrogen ion production mechanisms," Appl. Phys. Rev., vol. 2, p. 021305, jun 2015.

[24] W. Kraus, D. Wünderlich, U. Fantz, B. Heinemann, F. Bonomo, and R. Riedl, "Deuterium results at the negative ion source test facility ELISE," Cit. Rev. Sci. Instruments, vol. 89, may 2018.

[25] B. Heinemann, U. Fantz, W. Kraus, L. Schiesko, C. Wimmer, D. Wunderlich, F. Bonomo, M. Froschle, R. Nocentini, and R. Riedl, "Towards large and powerful radio frequency driven negative ion sources for fusion," New J. Phys., vol. 19, no. 1, 2017.

[26] V. Dudnikov, "Forty years of surface plasma source development," Rev. Sci. Instrum., vol. 83, no. 2, 2012.

[27] A. Rizzolo, M. Barbisan, L. Bizzotto, R. Capobianco, M. De Muri, M. Fadone, R. Ghiraldelli, S. Gorno, B. Laterza, G. Marchiori, D. Marcuzzi, L. Migliorato, F. Molon, D. Ravarotto, R. Rizzieri, F. Rossetto, E. Sartori, G. Serianni, and P. Veltri, "Characterization of the SPIDER Cs oven prototype in the CAesium Test Stand for the ITER HNB negative ion sources," Fusion Eng. Des., vol. 146, pp. 676–679, sep 2019.

[28] U. Kurutz, R. Friedl, and U. Fantz, "Investigations on Cs-free alternatives for negative ion formation in a low pressure hydrogen discharge at ion source relevant parameters," Plasma Phys. Control. Fusion, vol. 59, p. 075008, jul 2017.

[29] P. Kumar, A. Ahmad, C. Pardanaud, M. Carrère, J. M. Layet, G. Cartry, F. Silva, A. Gicquel, and R. Engeln, "Enhanced negative ion yields on diamond surfaces at elevated temperatures," J. Phys. D. Appl. Phys., vol. 44, no. 37, p. 372002, 2011.

[30] M. Bacal, "Negative hydrogen ion production in fusion dedicated ion sources," Chem. Phys., vol. 398, no. 1, pp. 3–6, 2012.

[31] J. Arianer, "Les sources de particules chargees," tech. rep., The Joint Universities Accelerator School, Geneva, Switzerland, 2004.

[32] U. Fantz and D. Wünderlich, "Franck–Condon factors, transition probabilities, and radiative lifetimes for hydrogen molecules and their isotopomeres," At. Data Nucl. Data Tables, vol. 92, pp. 853–973, nov 2006.

[33] T. Mosbach, "Population dynamics of molecular hydrogen and formation of negative hydrogen ions in a magnetically confined low temperature plasma," Plasma Sources Sci. Technol., vol. 14, no. 3, pp. 610–622, 2005.

[34] M. Capitelli, M. Cacciatore, R. Celiberto, O. De Pascale, P. Diomede, F. Esposito, A. Gicquel, C. Gorse, K. Hassouni, A. Laricchiuta, S. Longo, D. Pagano, and M. Rutigliano, "Vibrational kinetics, electron dynamics and elementary processes in H 2 and D 2 plasmas for negative ion production: modelling aspects," Nucl. Fusion, vol. 46, pp. 260–274, 2006.

[35] M. Capitelli, R. Celiberto, G. Colonna, F. Esposito, C. Gorse, K. Hassouni, A. Laricchiuta, and S. Longo, "Formation of Vibrationally and Rotationally Excited Molecules During Atom Recombination at Surfaces," in Fundam. Asp. Plasma Chem. Phys. - Kinet., pp. 57–78, Springer New York, 2016.

[36] W. Yang, S. N. Averkin, A. V. Khrabrov, I. D. Kaganovich, Y.-N. Wang, S. Aleiferis, and P. Svarnas, "Benchmarking and validation of global model code for negative hydrogen ion sources," Phys. Plasmas, vol. 25, no. 11, p. 113509, 2018.

[37] J. R. Hiskes, "Cross sections for the vibrational excitation of the H2 X 1Sigma g + (v) levels generated by electron collisional excitation of the higher singlet states," J. Appl. Phys., vol. 70, no. 7, pp. 3409–3417, 1991.

[38] J. R. Hiskes and A. M. Karo, "Recombination and dissociation of H2+ and H3+ ions on surfaces to form H2(v‘): Negative-ion formation on low-work-function surfaces," J. Appl. Phys., vol. 67, no. 11, pp. 6621–6632, 1990.

[39] B. Jackson and D. Lemoine, "Eley–Rideal reactions between H atoms on metal and graphite surfaces: The variation of reactivity with substrate," J. Chem. Phys., vol. 114, no. 1, p. 474, 2001.

[40]X. Sha, B. Jackson, and D. Lemoine, "Quantum studies of Eley–Rideal reactions between H atoms on a graphite surface," J. Chem. Phys., vol. 116, no. 16, p. 7158, 2002.
[41]S. Morisset, F. Aguillon, M. Sizun, and V. Sidis, "Quantum dynamics of H2 formation on a graphite surface through the Langmuir Hinshelwood mechanism," J. Chem. Phys., vol. 121, pp. 6493–6501, oct 2004.
[42]J. L. Lemaire, G. Vidali, S. Baouche, M. Chehrouri, H. Chaabouni, and H. Mokrane, "Competing Mechanisms of Molecular Hydrogen Formation in Conditions Relevant to the Interstellar Medium," Astrophys. J. Lett., vol. 725, no. 2, p. L156, 2010.
[43]M. Rutigliano and M. Cacciatore, "Eley-Rideal recombination of hydrogen atoms on a tungsten surface," Phys. Chem. Chem. Phys., vol. 13, no. 16, pp. 7475–7484, 2011.
[44]J. Harris and B. Kasemo, "On precursor mechanisms for surface reactions," Surf. Sci., vol. 105, pp. L281–L287, apr 1981.
[45]L. Gavilan, J. L. Lemaire, G. Vidali, T. Sabri, and C. Jæger, "The Formation of Molecular Hydrogen on Silicate Dust Analogs: The Rotational Distribution," Astrophys. J., vol. 781, no. 2, p. 79, 2014.
[46]M. Cacciatore and M. Rutigliano, "The semiclassical and quantum-classical approaches to elementary surface processes: dissociative chemisorption and atom recombination on surfaces," Phys. Scr., vol. 78, p. 058115, oct 2008.
[47]M. Cacciatore and M. Rutigliano, "Dynamics of plasma–surface processes: E–R and L–H atom recombination reactions," Plasma Sources Sci. Technol., vol. 18, p. 023002, may 2009.
[48]M. Rutigliano, M. Cacciatore, and G. Billing, "Hydrogen atom recombination on graphite at 10 K via the Eley–Rideal mechanism," Chem. Phys. Lett., vol. 340, pp. 13–20, may 2001.
[49]M. Bacal, A. A. Ivanov, M. Glass-Maujean, Y. Matsumoto, M. Nishiura, M. Sasao, and M. Wada, "Contribution of wall material to the vibrational excitation and negative ion formation in hydrogen negative ion sources (invited)," Rev. Sci. Instrum., vol. 75, no. 5, p. 1699, 2004.
[50]R. I. Hall, I. Čadež, M. Landau, F. Pichou, and C. Schermann, "Vibrational Excitation of Hydrogen via Recombinative Desorption of Atomic Hydrogen Gas on a Metal Surface," Phys. Rev. Lett., vol. 60, pp. 337–340, jan 1988.
[51]J. Bentounes, S. Béchu, F. Biggins, A. Michau, L. Gavilan, J. Menu, L. Bonny, D. Fombaron, A. Bès, Y. A. Lebedev, V. A. Shakhatov, P. Svarnas, T. Hassaine, J. L. Lemaire, and A. Lacoste, "Effects of the plasma-facing materials on the negative ion H- density in an ECR (2.45 GHz) plasma," Plasma Sources Sci. Technol., vol. 27, p. 055015, may 2018.
[52]S. Markelj and I. Čadež, "Production of vibrationally excited hydrogen molecules by atom recombination on Cu and W materials," J. Chem. Phys., vol. 134, no. 12, pp. –, 2011.
[53]Gough, S, Schermann, C, Pichou, F, Landau, M, Cadez, I, Hall, and I. R, "The formation of vibrationally excited hydrogen molecules on carbon surfaces," Astron. Astrophys., vol. 305, pp. 687–693, 1996.
[54]I. Cadez, R. I. Hall, M. Landau, F. Pichou, and C. Schermann, "Dissociative electron attachment to vibrationally excited H 2 and D 2 molecules: the 14 eV process," J. Phys. B At. Mol. Opt. Phys., vol. 21, no. 19, p. 3271, 1988.
[55]B. Xiao, S. Kado, S. Kajita, and D. Yamasaki, "Rovibrational distribution determination of H ₂ in low temperature plasmas by Fulcher- band spectroscopy," Plasma Phys. Control. Fusion, vol. 46, pp. 653–668, apr 2004.
[56]S. Briefi, D. Rauner, and U. Fantz, "Determination of the rotational population of H2 and D2 including high-N states in low temperature plasmas via the Fulcher-α transition," J. Quant. Spectrosc. Radiat. Transf., vol. 187, pp. 135–144, 2017.
[57]D. R. Farley, D. P. Stotler, D. P. Lundberg, and S. A. Cohen, "Modeling of hydrogen ground state rotational and vibrational temperatures in kinetic plasmas," J. Quant. Spectrosc. Radiat. Transf., vol. 112, no. 5, pp. 800–819, 2011.
[58]U. Fantz and B. Heger, "Spectroscopic diagnostics of the vibrational population in the ground state of H2 and D2 molecules," Plasma Phys. Control. Fusion, vol. 40, no. 12, p. 2023, 1998.
[59]B. P. Lavrov, A. A. Solov'ev, and M. V. Tyutchev, "Populations of the rotational levels of the d3-u levels of H2, HD, and D2 in an rf discharge," J. Appl. Spectrosc., vol. 32, pp. 316–320, apr 1980.
[60]B. P. Lavrov, V. N. Ostrovsky, and V. I. Ustimov, "Non-Franck-Condon transitions in the electron impact excitation of molecules. II. Semi-empirical approach: transitions in H2," J. Phys. B At. Mol. Phys., vol. 14, pp. 4701–4718, dec 1981.
[61]E. E. Marinero, C. T. Rettner, and R. N. Zare, "Quantum-state-specific detection of molecular hydrogen by three-photon ionization," Phys. Rev. Lett., vol. 48, pp. 1323–1326, may 1982.
[62]P. J. Eenshuistra, R. M. A. Heeren, A. W. Kleyn, and H. J. Hopman, "Dissociation and vibrational excitation of H2 molecules and wall influence on the densities in a multicusp ion," Phys. Rev. A, vol. 40, no. 7, pp. 3613–3625, 1989.
[63]E. E. Marinero, C. T. Rettner, R. N. Zare, and A. Kung, "Excitation of H2 using continuously tunable coherent XUV radiation (97.3-102.3 nm)," Chem. Phys. Lett., vol. 95, pp. 486–491, mar 1983.
[64]G. C. Stutzin, A. T. Young, H. F. Döbele, A. S. Schlachter, K. N. Leung, and W. B. Kunkel, "In situ density and temperature measurements of vibrationally excited hydrogen molecules in ion source plasmas," Rev. Sci. Instrum., vol. 61, pp. 619–621, jan 1990.
[65]G. Stutzin, A. Young, A. Schlachter, K. Leung, and W. Kunkel, "In situ measurement of rovibrational populations of H2 ground electronic state in a plasma by VUV laser absorption," Chem. Phys. Lett., vol. 155, pp. 475–480, mar 1989.
[66]D. Wagner, B. Dikmen, and H. F. Döbele, "Comparison of atomic and molecular densities and temperatures of deuterium and hydrogen plasmas in a magnetic multipole source," Plasma Sources Sci. Technol., vol. 7, no. 4, pp. 462–470, 1998.
[67]M. Pealat, J. P. E. Taran, M. Bacal, F. Hillion, M. Péalat, J. P. E. Taran, M. Bacal, and F. Hillion, "Rovibrational molecular populations, atoms, and negative ions in H[sub 2] and D[sub 2] magnetic multicusp discharges," J. Chem. Phys., vol. 82, no. 11, pp. 4943–4953, 1985.
[68]R. F. G. Meulenbroeks, R. A. H. Engeln, J. A. M. van der Mullen, and D. C. Schram, "Coherent anti-Stokes Raman scattering performed on expanding thermal arc plasmas," Phys. Rev. E, vol. 53, pp. 5207–5217, may 1996.
[69]K. Hassouni, G. Lombardi, A. Gicquel, M. Capitelli, V. A. Shakhatov, and O. De Pascale, "Nonequilibrium vibrational excitation of H2 in radiofrequency discharges: A theoretical approach based on coherent anti-Stokes Raman spectroscopy measurements," Phys. Plasmas, vol. 12, no. 7, p. 73301, 2005.
[70]T. Mosbach, H. M. Katsch, and H. F. Döbele, "Diagnostics in Plasmas of Electronic-Ground-State Hydrogen Molecules in High Vibrational and Rotational States by Laser-Induced Fluorescence with Vacuum-Ultraviolet Radiation," Phys. Rev. Lett., vol. 85, no. 16, pp. 3420–3423, 2000.
[71]P. Vankan, D. Schram, and R. Engeln, "High rotational excitation of molecular hydrogen in plasmas," Chem. Phys. Lett., vol. 400, pp. 196–200, dec 2004.
[72]O. Gabriel, D. C. Schram, and R. Engeln, "Formation and relaxation of rovibrationally excited H2 molecules due to plasma-surface interaction," Phys. Rev. E, vol. 78, no. 1, p. 16407, 2008.
[73]P. Schmidt, A. Hans, C. Ozga, P. Reiß, L. B. Ltaief, K. Hosaka, M. Kitajima, N. Kouchi, A. Knie, and A. Ehresmann, "Excitation-energy resolved fluorescence spectra of hydrogen molecules in the regime of singly excited molecular states," J. Phys. Conf. Ser., vol. 635, p. 112130, sep 2015.
[74]S. Béchu, S. Aleiferis, J. Bentounes, L. Gavilan, V. A. Shakhatov, A. Bès, P. Svarnas, S. Mazouffre, N. de Oliviera, R. Engeln, and J. L. Lemaire, "Detection of rovibrationally excited molecular hydrogen in the electronic ground state via synchrotron radiation," Appl. Phys. Lett., vol. 111, p. 074103, aug 2017.
[75]R. Agnello, S. Béchu, I. Furno, P. Guittienne, A. Howling,

R. Jacquier, G. Plyushchev, M. Barbisan, R. Pasqualotto, I. Morgal, and A. Simonin, "Negative ion characterization in a helicon plasma source for fusion neutral beams by cavity ring-down spectroscopy and Langmuir probe laser photodetachment," Nucl. Fusion, vol. 60, p. 026007, feb 2020.

[76]M. Berger, U. Fantz, S. Christ-Koch, and N. Team, "Cavity ring-down spectroscopy on a high power rf driven source for negative hydrogen ions," Plasma Sources Sci. Technol., vol. 18, p. 025004, may 2009.

[77]P. Sonato, P. Agostinetti, U. Fantz, T. Franke, I. Furno, A. Simonin, and M. Q. Tran, "Conceptual design of the beam source for the DEMO Neutral Beam Injectors," New J. Phys., vol. 18, no. 12, p. 125002, 2016.

[78]S. Aleiferis, P. Svarnas, S. Béchu, O. Tarvainen, and M. Bacal, "Production of hydrogen negative ions in an ECR volume source: balance between vibrational excitation and ionization," Plasma Sources Sci. Technol., vol. 27, p. 075015, jul 2018.

[79]S. Aleiferis, P. Svarnas, I. Tsiroudis, S. Bechu, M. Bacal, and A. Lacoste, "H- Negative Ion Production From a 2D Network of ECR Dipolar Plasma Sources," Plasma Sci. IEEE Trans., vol. 42, no. 10, pp. 2828–2829, 2014.

[80]S. Bechu, A. Soum-Glaude, A. Bes, A. Lacoste, P. Svarnas, S. Aleiferis, J. A. A. Ivanov, M. Bacal, S. Béchu, A. Soum-Glaude, A. Bès, A. Lacoste, P. Svarnas, S. Aleiferis, A. A. Ivanov Jr, and M. Bacal, "Multi-dipolar microwave plasmas and their application to negative ion production," Phys. Plasmas, vol. 20, no. 10, pp. 101601–101608, 2013.

[81]A. Lacoste, T. Lagarde, S. Béchu, Y. Arnal, J. Pelletier, S. Bechu, Y. Arnal, and J. Pelletier, "Multi-dipolar plasmas for uniform processing: physics, design and performance," Plasma Sources Sci. Technol., vol. 11, no. 4, p. 407, 2002.

[82]C. Marini, R. Agnello, B. P. Duval, I. Furno, A. A. Howling, R. Jacquier, A. N. Karpushov, G. Plyushchev, K. Verhaegh, G. Ph, U. Fantz, D. Wünderlich, S. Béchu, and A. Simonin, "Spectroscopic characterization of H 2 and D 2 helicon plasmas generated by a resonant antenna for neutral beam applications in fusion," Nucl. Fusion, vol. 57, no. 3, p. 36024, 2017.

[83]B. J. Wood and H. Wise, "Diffusion and Heterogeneous Reaction. II. Catalytic Activity of Solids for Hydrogen-Atom Recombination," J. Chem. Phys., vol. 29, no. 6, pp. 1416–1417, 1958.

[84]B. J. Wood and H. Wise, "Kinetics of hydrogen atom recombination on surfaces," J. Phys. Chem., vol. 65, no. 11, pp. 1976–1983, 1961.

[85]F. Taccogna, R. Schneider, S. Longo, M. Capitelli, F. Tccogna, R. Schneider, S. Longo, and M. Capitelli, "Modeling of a negative ion source. I. Gas kinetics and dynamics in the expansion region," Phys. Plasmas, vol. 14, no. 7, p. 73503, 2007.

[86]N. de Oliveira, D. Joyeux, D. Phalippou, J. C. Rodier, F. Polack, M. Vervloet, and L. Nahon, "A Fourier transform spectrometer without a beam splitter for the vacuum ultraviolet range: From the optical design to the first UV spectrum," Rev. Sci. Instrum., vol. 80, p. 043101, apr 2009.

[87]N. de Oliveira, M. Roudjane, D. Joyeux, D. Phalippou, J.-C. Rodier, and L. Nahon, "High-resolution broad-bandwidth Fourier-transform absorption spectroscopy in the VUV range down to 40 nm," Nat. Photonics, vol. 5, pp. 149–153, mar 2011.

[88]N. de Oliveira, D. Joyeux, M. Roudjane, J.-F. Gil, B. Pilette, L. Archer, K. Ito, L. Nahon, and IUCr, "The high-resolution absorption spectroscopy branch on the VUV beamline DESIRS at SOLEIL," J. Synchrotron Radiat., vol. 23, pp. 887–900, jul 2016.

[89]G. D. Dickenson, T. I. Ivanov, W. Ubachs, M. Roudjane, N. De Oliveira, D. Joyeux, L. Nahon, W. Ü. L. Tchang-Brillet, M. Glass-Maujean, H. Schmoranzer, A. Knie, S. Kbler, and A. Ehresmann, "VUV spectroscopic study of the D 1 II u state of molecular deuterium," Mol. Phys., vol. 109, pp. 2693–2708, nov 2011.

[90]M. Eidelsberg, J. L. Lemaire, S. R. Federman, G. Stark, A. N. Heays, Y. Sheffer, L. Gavilan, J.-H. Fillion, F. Rostas, J. R. Lyons, P. L. Smith, N. de Oliveira, D. Joyeux, M. Roudjane, and L. Nahon, "High-resolution study of oscillator strengths and predissociation rates for ¹² C ¹⁶ O," Astron. Astrophys., vol. 543, p. A69, jul 2012.

[91]J.-Y. Roncin, F. Launay, J.-Y. Roncin, and F. Launay, "Atlas of the vacuum ultraviolet emission spectrum of molecular hydrogen," Atlas Vac. Ultrav. Emiss. Spectr. Mol. Hydrog. /Jean-Yves Roncin Fr. Launay. Washingt., 1994.

[92]G. Sultan, G. Baravian, M. Gantois, G. Henrion, H. Michel, and A. Ricard, "Doppler-broadened Hα line shapes in A dc low-pressure discharge for TiN deposition," Chem. Phys., vol. 123, no. 3, pp. 423–429, 1988.

[93]N. SADEGHI, "6. Molecular Spectroscopy Techniques Applied for Processing Plasma Diagnostics," J. Plasma Fusion Res., vol. 80, no. 9, pp. 767–776, 2004.

[94]A. Rousseau, E. Teboul, and N. Sadeghi, "Time-resolved gas temperature measurements by laser absorption in a pulsed microwave hydrogen discharge," Plasma Sources Sci. Technol., vol. 13, no. 1, pp. 166–176, 2004.

[95]O. Gabriel, J. J. A. van den Dungen, D. C. Schram, and R. Engeln, "Nonequilibrium rovibrational energy distributions of hydrogen isotopologues in an expanding plasma jet," J. Chem. Phys., vol. 132, no. 10, p. 104305, 2010.

[96]K. J. Chung, J. J. Dang, J. Y. Kim, W. H. Cho, and Y. S. Hwang, "Kinetics of electrons and neutral particles in radio-frequency transformer coupled plasma H- ion source at Seoul National University," New J. Phys., vol. 18, p. 105006, oct 2016.

[97]S. Christ-Koch, U. Fantz, and M. Berger, "Laser photodetachment on a high power, low pressure rf-driven negative hydrogen ion source," Plasma Sources Sci. Technol., vol. 18, no. 2, 2009.

[98]A. A. Matveyev and V. P. Silakov, "Kinetic processes in a highly-ionized non-equilibrium hydrogen plasma," Plasma Sources Sci. Technol., vol. 4, no. 4, p. 606, 1995.

[99]C. Gorse, M. Capitelli, M. Bacal, J. Bretagne, and A. Laganà, "Progress in the non-equilibrium vibrational kinetics of hydrogen in magnetic multicusp H- ion sources," Chem. Phys., vol. 117, pp. 177–195, oct 1987.

[100]M. Bacal, "Volume Generation of H- Ions in Plasmas," Phys. Scr., vol. T2B, pp. 467–478, 1982.

[101]J. R. Hiskes, A. M. Karo, M. Bacal, A. M. Bruneteau, and W. G. Graham, "Hydrogen vibrational population distributions and negative ion concentrations in a medium density hydrogen discharge," J. Appl. Phys., vol. 53, pp. 3469–3475, may 1982.

[102]J. R. Hiskes, "Cross sections for the vibrational excitation of the H2(X 1 sigma) state via electron collisional excitation of the higher singlet states," J. Appl. Phys., vol. 51, pp. 4592–4594, sep 1980.

[103]A. M. Karo, J. R. Hiskes, and R. J. Hardy, "Vibrational relaxation in H 2 molecules by wall collisions: Applications to negative ion source processes," J. Vac. Sci. Technol. A Vacuum, Surfaces, Film., vol. 3, pp. 1222–1228, may 1985.

[104]P. J. Eenshuistra, J. H. M. Bonnie, J. Los, and H. J. Hopman, "Observation of Exceptionally High Vibrational Excitation of Hydrogen Molecules Formed by Wall Recombination," Phys. Rev. Lett., vol. 60, pp. 341–344, jan 1988.